ORIGINAL RESEARCH **Open access**

Detection of Maize Lodging Through Canopy Structural Similarity Analysis Using UAV LiDAR

James O'Leary[1*], Aisling Dunne[1], Sean O'Brien[2], Niamh Ryan[3]

Abstract

Lodging represents a substantial obstacle in maize cultivation, seriously hindering both yield advancement and the productivity of mechanical harvesting. Contemporary farming regimes, marked by dense crop stands and multi-cultivar intercropping, urgently require the development of accurate, rapid sensing methods to manage lodging problems. In the present work, an unmanned aerial vehicle (UAV) equipped with a light detection and ranging (LiDAR) sensor was deployed to acquire high-fidelity point cloud data of fully mature field maize. A novel technique was proposed that autonomously pinpoints structural divergences triggered by lodging by evaluating canopy structural resemblance across stratified height bands within the point cloud. This pipeline permits unattended detection of maize lodging in heterogeneous field settings. The experimental outcomes illustrate that: (1) High-fidelity point cloud information effectively registers lodging-induced alterations in canopy architecture. Through the structural similarity change curve, the vertical threshold for lodging can be determined without human input (best threshold: 1.76 m), yielding a mere 2.3% divergence between the algorithm-derived lodging footprint and the manually surveyed reference (ground truth); (2) A sensitivity test of the vertical threshold indicates that when this value oscillates by ± 5 cm (1.71–1.81 m), the error in lodging area estimation stays below 10% (peak error = 8.2%), confirming marked robustness of the autonomously selected parameter; (3) While UAV flight elevation exerts an influence on point cloud fidelity (e.g., low flight: 25 m, high flight: 80 m), the vertical cutoff derived from low-elevation surveys can, to a degree, be transferred to high-elevation monitoring. In the current study, this transfer led to an area estimation discrepancy of only 5.3%.

Keywords Maize, UAV-LiDAR, Height threshold, Automated lodging monitoring, Point cloud

*Correspondence:
James O'Leary
james.oleary@ucd.ie
[1] Department of Artificial Intelligence for Grassland and Pasture Management, School of Agriculture, University College Dublin, Dublin, Ireland
[2] Department of Machine Learning for Fertilizer Recommendation Systems, School of Agriculture, University of Limerick, Limerick, Ireland
[3] Department of Smart Grazing Rotation Planning, Faculty of Agriculture, University of Galway, Galway, Ireland

Introduction

As a staple food crop of global significance, maize suffers annual productivity losses in the range of about 13% to 50% attributable to lodging—a major biotic/abiotic constraint characterized by the irreversible buckling or leaning of stalks away from the upright orientation, commonly instigated by wind force, heavy precipitation, or pest damage, which gravely impairs crop output [1-3]. The widespread adoption of advanced agronomic techniques, including elevated planting densities and mixed-species cultivation, increases the likelihood of lodging by weakening stem anchorage and reducing within-canopy air movement [4, 5]. Reliable and prompt extraction of lodging-relevant metrics across intricate farming landscapes thus becomes indispensable for facilitating preemptive field interventions, streamlining insurance loss adjustment, and reinforcing yield prediction models [6, 7].

This is an open access article distributed under the terms of the Creative Commons Attribution-NonCommercial-ShareAlike 4.0 International License (CC BY-NC-SA 4.0), which permits non-commercial use, distribution, reproduction, and adaptation in any medium or format, provided that appropriate credit is given to the original author(s) and source, a link to the license is provided, and any changes made are indicated. Adapted material must be distributed under the same license.

© 2023 The Author(s). | Published by Agro Intelligence Research Press

Ground-based manual surveying has historically constituted the cornerstone technique for lodging assessment. Such conventional tactics are, however, markedly constrained when applied to extensive farmland tracts, since they impose heavy labor demands—especially in regions susceptible to recurrent disasters—and routinely involve timelines stretching from weeks to months from field data capture through to analytical outputs [8, 9]. This protracted cycle renders the accurate capture of the brief, decisive interval during which lodging occurs nearly impossible [10, 11]. The advent of remote sensing has fundamentally reshaped this discipline. Unmanned aerial vehicle (UAV) systems, in particular, which afford centimeter-level imagery, operational versatility, and potential for multisensor integration [12, 13], have demonstrated substantial utility in deriving multi-tier lodging characteristics from crop stands [14, 15]. A distinguishing virtue of UAV-centric remote sensing is its ability to rapidly acquire high-fidelity spectral signatures and detailed three-dimensional structural parameters of affected vegetation [16]. Concretely, LiDAR instruments enable rigorous measurement of crop inclination and lodging severity by generating fine-scale digital terrain models (DTMs) and crop height maps. The expanding corpus of scholarship in recent years dedicated to UAV remote sensing of crop lodging attests to the wide-ranging and encouraging trajectory of these technological developments.

Prevailing research predominantly focuses on identifying lodging-induced signatures in RGB and multispectral imagery. Among the notable scholarly contributions, the work by Zhang *et al.* [17] deserves particular mention. These authors pioneered the application of the deep-learning architecture GoogLeNet to UAV-acquired high-resolution RGB images, successfully teasing apart nuanced morphological cues separating lodged from erect plants. By conditioning their model to internalize these subtle distinctions, the investigators attained high-accuracy detection of wheat lodging. Yet, reliance solely on RGB channels may prove inadequate for detecting the challenges posed by heterogeneous field backdrops. The research group of Li *et al.* [18] broadened the scope of investigation by exploring the utility of near-infrared (NIR) spectral bands, revealing that combining NIR information with visible imagery could markedly improve the fidelity of sunflower lodging classification. Specifically, deploying the SegNet architecture on the integrated RGB + NIR data stack delivered an overall accuracy of 88.23%, comfortably outstripping classical machine learning classifiers. This finding signals that multimodal data amalgamation can partially compensate for the deficiencies inherent in single-source inputs. Beyond spectral content, the three-dimensional architectural attributes of vegetation represent another critical dimension for lodging surveillance. The study of Guan *et al.* [19] serves as an illustrative case: they reconstructed a canopy height model (CHM) from UAV stereoscopic pairs. They coupled it with multispectral vegetation indices to assemble a composite feature pool for maize lodging. When these variables were subjected to the random forest classifier, the team achieved a global recognition accuracy of 95%. In a similar vein, Sun *et al.* [20] employed maximum-likelihood classification on feature ensembles and effectively discriminated varying severities of maize lodging, powerfully underscoring the operational value of UAV-borne multispectral imagery.

While a substantial body of work has borne out the effectiveness of UAV remote sensing for lodging surveillance, current paradigms still exhibit several shortcomings. On one front, the extraction of discriminatory features—including spectral reflectance patterns and textural signatures of lodged crops—is contingent upon supervised classification pipelines. These frameworks require extensive annotation of exemplar samples to adequately represent lodging-related spectral-geometric attributes, thereby increasing the cost of model construction. Compounding this issue, modern agronomic systems frequently deploy multi-cultivar, multi-density intercropping arrangements. Plants within lodging-affected patches often exhibit pronounced disparities in both stand density and varietal identity, further magnifying the difficulty and cost of sample annotation [21, 22]. On another front, visible-spectrum imaging operates on optical appearance and is acutely sensitive to fluctuating illumination conditions and soil background clutter. It is frequently the case that the boundaries of lodged zones are difficult to define with precision, introducing additional obstacles to faithful labeling. While multispectral sensors can relay information on crop physiological condition (via proxies such as NDVI), their comparatively coarse spatial resolution necessitates pairing with advanced machine learning frameworks to indirectly infer lodging status. Such a strategy renders the quantitative grading of lodging severity especially problematic [23, 24].

In contrast, LiDAR technology offers a more straightforward approach, leveraging three-dimensional point clouds to directly measure crop deviation angles, height compression, and the spatial extent of lodging, thereby supporting both visual interpretation and quantitative grading of lodging magnitude. Plant stature, as a pivotal structural descriptor,

© 2023 The Author(s). | Published by Agro Intelligence Research Press

supplies auxiliary information that enhances spectral-based approaches. Miao *et al.* [25] demonstrated that integrating height metrics improves the precision with which crop lodging can be geolocated and delineated, particularly enhancing assessment reliability in complex field conditions. Moreover, the analyses by Refs. [26, 27] underscore that future trajectories in UAV remote sensing should pivot toward the synergistic fusion of multidimensional data streams to realize higher levels of intelligent situational awareness.

Crop lodging is a prevalent biological event in which formerly upright vegetation inclines or collapses under the influence of various endogenous and exogenous factors [28, 29]. Across the phenotypic indicators enlisted to diagnose lodging, a conspicuous reduction in standing height ranks among the most immediately observable cues [30-32]. Relative to intricate optical image attributes such as hue and texture, plant height—as a straightforwardly measurable morphological variable—affords distinctive benefits for adjudicating crop lodging condition [33]. Foundational investigations have long substantiated the instrumental role of plant height data in reliably flagging lodging [34, 35]. By way of illustration, Zhou *et al.* [36] flew a UAV equipped with a Riegl VUX-1 LiDAR and captured a canopy-height profile of lodged maize with high reliability. By contrasting the stature of unaffected and impacted plants, they verified that height measurements faithfully reflect the severity of lodging. Likewise, Chu *et al.* [37] operated a compact UAV platform combining RGB and near-infrared imagers to corroborate a tight correlation between remotely estimated and field-measured height figures.

Furthermore, Hu *et al.* [38] performed a comparative evaluation across three data acquisition modalities: UAV lidar, portable backpack lidar, and a three-dimensional reconstruction derived from UAV digital photographs, concluding that UAV lidar delivers superior performance for maize lodging monitoring. Taken together, these studies reassert the centrality of plant height in multi-faceted lodging assessment. It warrants emphasis, however, that although these investigations impart valuable insights, their applicability remains fairly circumscribed, and the specification of height cutoffs continues to rely heavily on subjective expert judgement. Realizing self-adaptive lodging monitoring guided by height thresholds that deliver accurate appraisals amid the complexity of modern agricultural cropping systems remains an urgent and unresolved research gap [39, 40].

Given the intrinsic constraints of traditional optical remote sensing in acquiring plant height data, UAV LiDAR technology is a highly efficient and metrologically rigorous means of three-dimensional data acquisition [41]. It can resolve minute disparities in crop canopy architecture with exceptional fidelity, even under complex field conditions [42, 43]. This edge becomes particularly manifest when surveying tall-statured cereals such as maize. Within this framework, an automated diagnostic procedure grounded on height thresholds carries considerable practical merit. By judiciously setting height cutoffs, LiDAR technology can rapidly pinpoint vegetated areas where height falls outside the normative range, thereby facilitating accurate recognition of lodging events. The principal strength of this paradigm lies in its potential to dramatically increase throughput while sharply curtailing reliance on human intervention, thereby providing an actionable solution for the stewardship of expansive agricultural holdings.

The present inquiry is designed to undertake an exhaustive examination of canopy architectural variability across inter-planting regimes encompassing multiple maize hybrids and population densities, drawing on LiDAR-equipped unmanned aerial vehicle (UAVs) point cloud data. Addressing the limitation that existing height-threshold-based lodging extraction protocols are overly reliant on domain expertise, this investigation introduces an adaptive methodology for determining height cutoffs. This technique intends to facilitate unattended monitoring and rigorous quantification of maize lodging conditions within complex farmland mosaics, thereby enhancing the flexibility and field-level utility of UAV LiDAR systems in authentic agricultural contexts. The central research thrusts of this paper are dual: (1) Methodological Construction: Devise an automated algorithmic pipeline for efficient maize lodging detection from LiDAR point clouds through self-tuning height threshold identification. (2) Validation and Refinement: Corroborate the precision of the proposed method and methodically probe the effects of variables such as flight altitude and threshold perturbations on its efficacy, to safeguard its stability and dependability under a spectrum of environmental circumstances.

The rest of this article is structured in the following manner. Section 2 delineates the study site and datasets, together with the technical specifics of the introduced adaptive height threshold selection algorithm. Section 3 reports the experimental

© 2023 The Author(s). | Published by Agro Intelligence Research Press

outcomes and furnishes a comprehensive appraisal of the method's resilience. Section 4 scrutinizes the bearing of core parameters on the correctness and broad transferability of the approach. To conclude, Section 5 synthesizes the principal discoveries and elaborates on their practical ramifications.

Materials and Methods

Overview of the study area

Fieldwork was performed at the Experimental Demonstration Base of the National Maize Industrial Technology System situated in Xinzhou City, Shanxi Province, China **(Figure 1)**. Representing a major agricultural hub in North China, Xinzhou lies within a temperate continental monsoon climate, with pronounced seasonal contrasts that provide near-optimal conditions for maize cultivation. The locality's mean annual temperature oscillates between 4.3 °C and 9.2 °C, yearly precipitation totals vary from 345 mm to 588 mm, and the annual duration of sunshine extends from 2400.9 to 2911.3 h. This propitious convergence of thermal input, water availability, and solar radiation has forged Xinzhou's single-crop-per-year farming calendar, an arrangement well-adapted to the inherent agro-climatic constraints. Such a monocropping paradigm aligns closely with the regional endowment of natural resources, enabling efficient use of climatic potential for maize output.

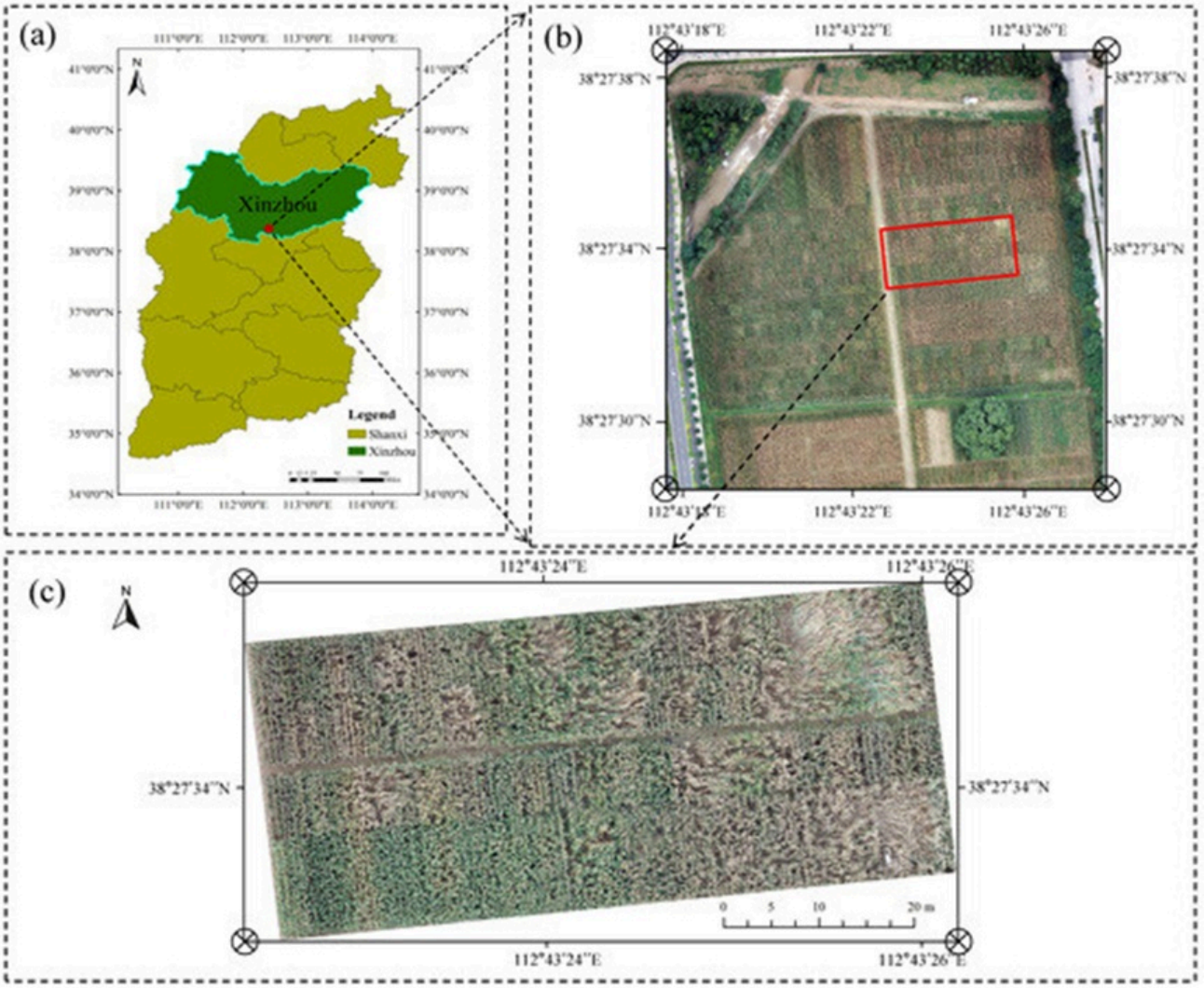

© 2023 The Author(s). | Published by Agro Intelligence Research Press

Figure 1. (a) The geographical location of Xinzhou City, (b) Geospatial distribution of research focus areas, and (c) The spatial distribution of maize experimental fields in the study area.

Two experimental sectors (Experimental Area 1 and Experimental Area 2) were demarcated within the field site. As illustrated in **Figure 2**, differing configurations were applied to the two sectors with respect to maize genotypes and stand densities. Across Experimental Area 1, a pair of population densities was imposed: 8 plants/m² together with 10 plants/m². For each density treatment, 30 individual plots (6 m × 6 m) were established. These units were aligned north–south and split into three replicate clusters, each comprising 10 plots. Every plot hosted two maize types. Irrespective of density level, the varieties were ordered along a west-to-east transect, comprising 10 genotypes: MC 703, Jiushenghe 2468, Ruipu 909, Xinyu 108, Lianchuang 825, Shandan 650, Kehe 699, Qiangsheng 388, Xianyu 335, and Zhengdan 958. Within Experimental Area 1, these entries were concisely relabeled A1 through A10, in the same sequence. Turning to Experimental Area 2, a set of 10 plots was laid down, each covering an extent of 6 m × 10 m. The design encompassed five graduated planting density levels: 4 plants/m², 6 plants/m², 7 plants/m², 9 plants/m², and 10 plants/m², along with a pair of maize genotypes: Zhengdan 958 and Xianyu 335. In particular, Zhengdan 958 received the identifier "A10" within Experimental Area 2, while Xianyu 335 was tagged as "A9". It is worth noting that distinct maize genotypes exhibit divergent terminal heights at physiological maturity. The field-surveyed average statures of the respective genotypes are catalogued in **Table 1**.

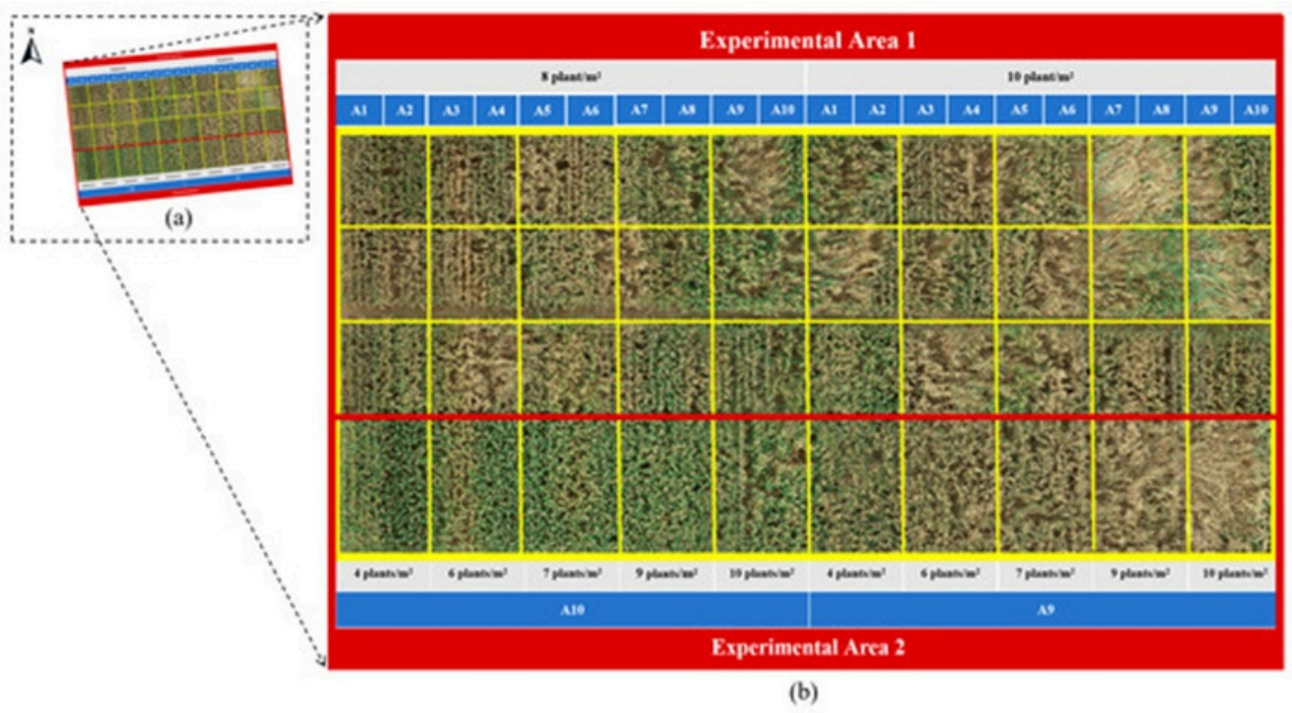

Figure 2. (a) Distribution of planting varieties and planting densities in the maize experimental field, and (b) Visualization of **Figure 2a** after rotation and enlargement.

Table 1. Maize varieties and their respective plant heights.

Maize variety name	Average plant height (cm)	Variety abbreviation
MC 703	310	A1
Jiushenghe 2468	298	A2
Ruipu 909	286	A3

© 2023 The Author(s). | Published by Agro Intelligence Research Press

Xinyu 108	318	A4
Lianchuang 825	301	A5
Shandan 650	277	A6
Kehe 699	350	A7
Qiangsheng 388	332	A8
Xianyu 335	319	A9
Zhengdan 958	277	A10

Image collection from UAV platforms

Field measurements were gathered via two principal instrument suites: a UAV-borne LiDAR rig and a UAV-mounted visible-spectrum camera rig. As portrayed in **Figure 3a**, the LiDAR rig couples a DJI Matrice 600 Pro UAV (Da-Jiang Innovations, Shenzhen, China) with a Hummingbird Genius compact LiDAR scanner (SureStar, Beijing, China). Its defining technical specifications are compiled within **Table 2**. In the context of this work, the longitudinal and lateral overlap fractions were set to 40% to preserve the wholeness and seamless continuity of the point cloud record; the craft was piloted at 25 m above ground with a traversal speed of 3 m/s, balancing point density and mission duration. As shown in **Figure 3b**, the visible-spectrum imaging rig used a DJI Phantom 4 Pro UAV (Da-Jiang Innovations, Shenzhen, China) carrying a 1-inch CMOS detector with an 84° wide-angle optic. The sensor resolves 4864 × 3648 pixels and achieves a ground sampling distance (GSD) of just 7.2 mm, enabling the capture of exceedingly nuanced image textures. To further enhance image fidelity, the along-track and cross-track overlap fractions for the optical rig were set to 80%—a parameterization selected to improve the accuracy of the subsequent orthomosaic assembly.



Figure 3. (a) The UAV LiDAR system, and (b) The UAV visible light imaging system.

Table 2. LiDAR system parameters.

Parameters	Values
Laser wavelength	905 nm
Measurement rate	320 kHz
Maximum range	200 m
Field of view	360° × ±15°

© 2023 The Author(s). | Published by Agro Intelligence Research Press

Echo number	2 (first and last)
Range Accuracy	2 cm

Preconditioning the UAV LiDAR measurements primarily entails three central stages: data reduction, point cloud co-registration, and point cloud filtering. Data reduction subsumes two vital operations: fused processing of Global Navigation Satellite System (GNSS) observables with Inertial Measurement Unit (IMU) streams to reconstruct the flight trajectory, and the derivation of LiDAR point returns. Within this study, the POSPac UAV 8.3 Lite application suite was tasked with trajectory estimation, while the StarSolve software (v2021) was responsible for LiDAR point extraction. Co-registration of the point cloud was performed using the Align routine in CloudCompare (v2.13.2). To cleanse the raw cloud, a Statistical Outlier Removal (SOR) sieve was deployed to excise noise points, succeeded by the application of the Cloth Simulation Filtering (CSF) procedure to segregate terrain strikes from above-ground strikes. Targeted effort was devoted to stripping ground echoes from the walkway traversing the experimental field, ensuring that the final point cloud corpus captured, above all, the canopy architecture of the maize crop. Owing to the modest spatial footprint and broadly planar relief of the investigation locale, the lowest elevation in the cloud was used as the ground reference plane. A height-differencing operation was then invoked to derive the Canopy Height Model (CHM), with the attendant benefit of reduced processing burden. All data-handling sequences were carried through within the CGCS2000/6-degree zone Gauss-Krüger projected coordinate framework (central meridian: 111° E) to ensure spatial coherence throughout the dataset. **Figure 4** presents the stepwise preprocessing pipeline for the point cloud data, culminating in the production of the field-level datasets necessary for the present investigation.

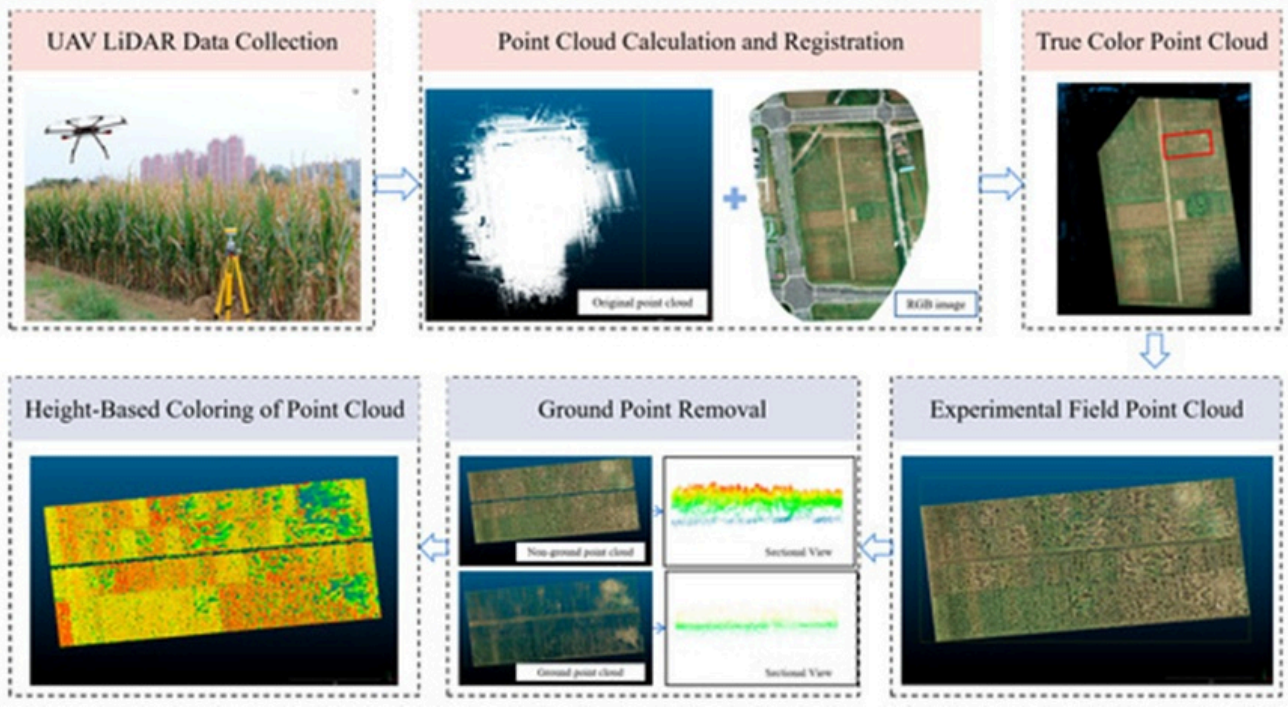

Figure 4. Sequential acquisition process of the point cloud data used in the experiment.

Implementation of the adaptive height threshold algorithm

This contribution proposes an unsupervised method for determining a height threshold from canopy point cloud data, assuming a level ground surface. The procedural architecture of the introduced tactic is sketched in **Figure 5** and expounded in detail hereafter:

© 2023 The Author(s). | Published by Agro Intelligence Research Press

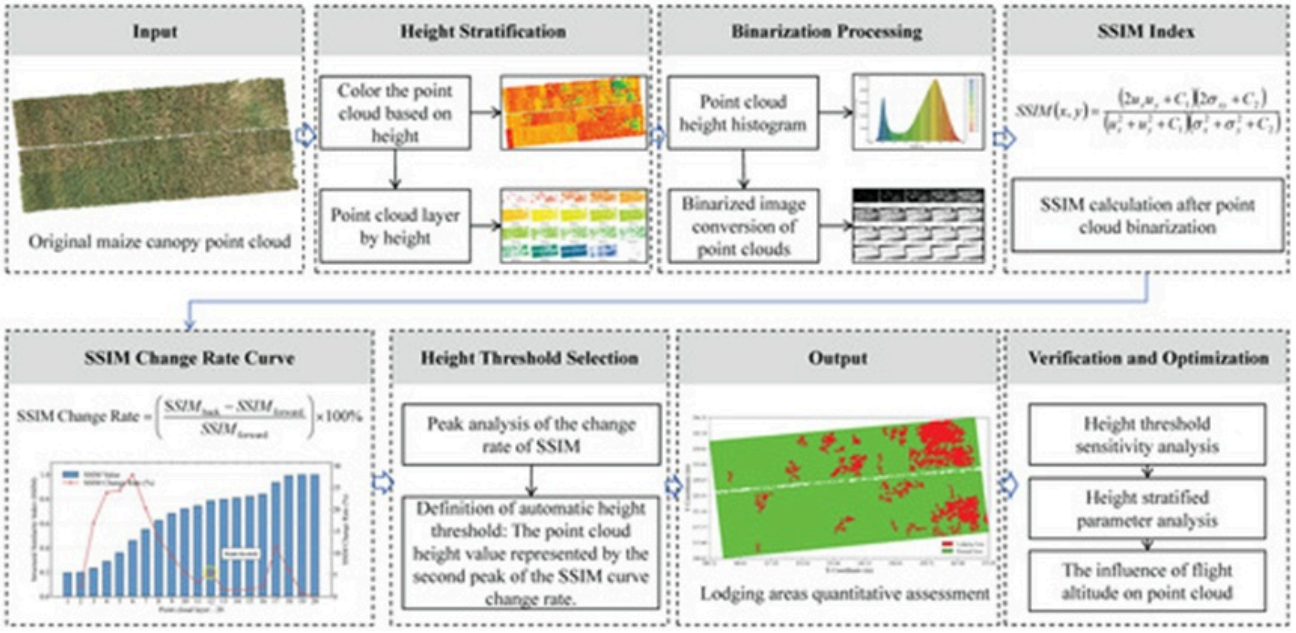

Figure 5. Flowchart of the proposed adaptive height threshold selection method.

Height Stratification: At the outset, this tactic segments the raw point cloud into evenly spaced height bands based on its vertical position attribute, decomposing the intricate volumetric point cloud.

Binarization Processing: After height stratification, the point cloud slices are cumulated band by band in a top-down sequence and rendered into binary image masks. This binarization step sharpens feature detectability by clearly outlining the borders of lodged patches whilst concurrently removing a large fraction of superfluous data, thereby elevating computational speed.

SSIM: To achieve a more rigorous appraisal of the correspondence between stratified point cloud levels and the full dataset, the Structural Similarity Index (SSIM) [44, 45] is incorporated as a key evaluation criterion. SSIM, a widely adopted metric for image fidelity measurement, gauges the degree of likeness between two images by comparing their luminance distributions, contrast characteristics, and structural patterns. In the devised workflow, SSIM is tasked with computing the resemblance linking binary masks generated from stratified point accumulations and the binary mask produced straightforwardly from the unstratified original point cloud. This stratagem simultaneously gauges the affinity of each stratified band relative to the overarching dataset and reveals fine-grained fluctuations across the vertical spectrum.

SSIM Change Rate Curve: The rate of fluctuation in SSIM magnitudes—formalized as the relative percentage shift between consecutive SSIM indices—undergoes subsequent examination. The resultant curve of change rates provides a graphical representation of the structural transformations inherent in the point cloud ensemble and lays a principled groundwork for height-cutoff determination. Through charting and interrogation of this curve, the kinetic signatures of structural reconfiguration across height strata emerge distinctly. Local maxima along the curve frequently align with abrupt structural ruptures, potentially indicative of lodging episodes.

Selection of the height threshold: Ultimately, by scrutinizing the distribution of peaks along the SSIM change rate curve, the vertical cutoff for lodging adjudication is pinpointed as the point cloud elevation value corresponding to the second local maximum.

Verification and optimization: To corroborate both the correctness and robustness of the proposed procedure, the introduced framework also includes a high-threshold sensitivity audit. Furthermore, it rigorously explores the extent to

© 2023 The Author(s). | Published by Agro Intelligence Research Press

which parameters, such as the fineness of the point cloud height stratification and the platform flight elevation, modulate performance, thereby ensuring the technique's transferability and reliability under heterogeneous ambient conditions.

Results and Discussion

Analysis of lodging situation in the study area

Maize canopy stature serves as an immediate and faithful proxy for crop developmental condition, as it directly reflects the vigor and ontogenetic progress of maize individuals. To render the spatial arrangement of canopy elevation visually explicit, a chromatic encoding protocol was applied to the point cloud. Concretely, individual returns were assigned separate colors based on their vertical coordinate: blue indicates the zones of minimal height, followed by green (slightly taller), yellow (intermediate elevation), and red (maximal height). The outcomes following this treatment are showcased in **Figure 6a**. Through visual inspection of point cloud chromatic gradients, lodging patches—chiefly exhibiting blue and green tonalities—can be identified with dispatch. These lodged sectors display uneven morphological outlines, and the marked color discontinuities further accentuate the diversity in lodging magnitude and typology. The sharply delineated color transitions not only aid swift recognition of lodging-impacted zones but additionally unveil the spatially heterogeneous makeup of lodging manifestations across the study domain.

© 2023 The Author(s). | Published by Agro Intelligence Research Press

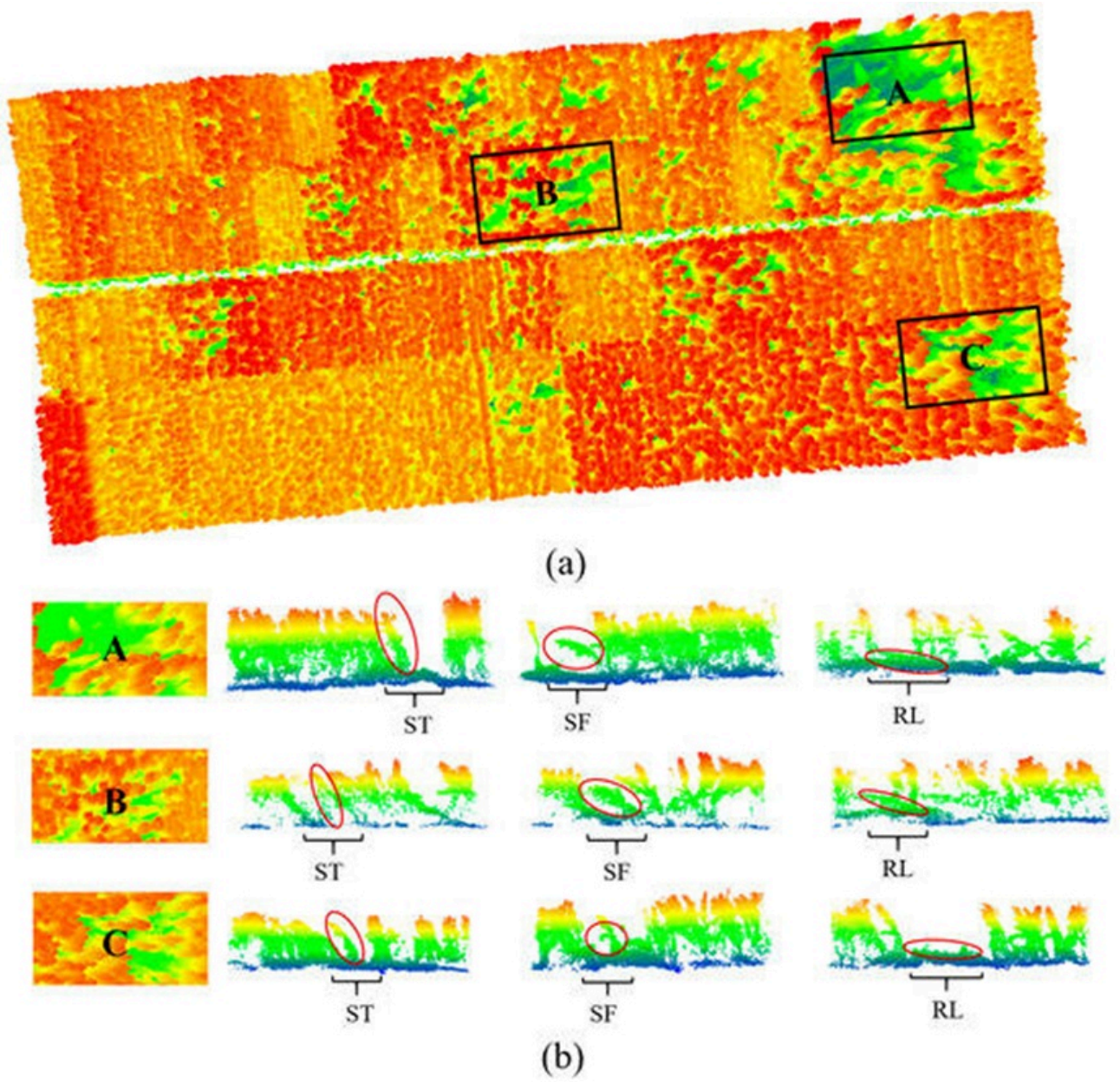

Figure 6. (a) Experimental field point cloud data colored by height, and (b) Point cloud profile of the lodging area. Note: ST: stem tilt; SF: stem folding; RL: root lodging.

As depicted in **Figure 6b**, three illustrative zones predisposed to lodging were located within the investigative area, labeled A, B, and C correspondingly. To achieve a fuller characterization of the vertical spread signatures inherent in the point cloud, lengthwise cross-sectioning was performed on the LiDAR measurements—a strategy aimed at visually grasping the volumetric configuration of maize specimens, thereby supporting the classification of lodging magnitude and form. In maize specimens in a sound, upright developmental stance, the point cloud exhibited a well-proportioned chromatic spectrum (spanning red to blue), reflecting uniform, upright elongation. By way of contrast, lodging episodes were betrayed by striking aberrations in both the chromatic constitution and the return compactness of the cloud. According to the scale of plant deviation, lodging was divided into three groupings: light lodging (marked by gentle stalk leaning devoid of full toppling), medium lodging (defined by entire stalk prostration level with the ground), and extreme lodging (distinguished by root severance from the earth substrate). A close examination of the three pinpointed lodging pockets revealed pronounced, gradient-guided differences in point cloud architecture, which mapped cleanly onto the

© 2023 The Author(s). | Published by Agro Intelligence Research Press

varying severities of lodging. These findings provide empirical support for the practicality of using UAV-carried LiDAR for maize lodging tracking, as the point cloud accurately captured the spatial characteristics of lodging across a range of intensities.

From the standpoint of point cloud cross-sectional properties, the trio of lodging forms displays sharply discernible hallmarks. Stem tilt (ST) announces itself through a lessening of aggregate plant point cloud elevation, whilst partly safeguarding the upright chromatic run (e.g., red to blue). The point cloud shows fairly high compactness and architectural linkage, suggesting that stalks are slanted at some angle without total rupture or flat collapse. Stem folding (SF) declares itself through an abrupt nosedive of canopy altitude, the obliteration of topmost returns (customarily red), and the massing of returns into irregularly dense clumps at depressed heights—consonant with stalk buckling/breakage deranging canopy structure. Root lodging (RL) puts forward the most disaggregated point cloud configuration: aggregate stature plunges catastrophically to virtually ground-level bands, swamped by blue and green low-position returns. The thinned point cloud shows increased spatial scatter without any distinguishable plant outlines, an aftermath of specimens reclining flat after root disengagement. The inquiry at hand concentrates on a pair of severe lodging manifestations: stem folding (SF) alongside root lodging (RL). Compared with stem tilt (ST), both SF and RL exhibit more pronounced spatial architectural disruption. Their stark structural imprints simplify detection and delineation within point cloud corpuses, furnishing high-relief signatures for unassisted recognition.

Automated selection of height thresholds

Accepting that the fundamental divergence between lodged and ordinarily developing sectors lies in canopy stature, enlisting a vertical cutoff for separation is a potent and straightforward approach. Via the utilization of a point cloud height stratification procedure, which consists of carving up the volumetric point cloud corpus into seamless horizontal slices following the vertical axis, plus subsequent scrutiny of point cloud arrangement properties inside these separate height intervals, the delicate fluctuation hallmarks of the vertical framework of field-grown maize can be veraciously registered and gauged. Such stratification not only reveals the presence or absence of vegetation at given altitudes but also illuminates the crowding and spatial ordering of returns, which serve as cardinal telltales of structural soundness and lodging intensity. **Figure 7a** schematically depicts the point cloud configuration across the investigative domain after height stratification. In this portrayal, each horizontal slice corresponds to the spatial scatter of returns confined to a particular height band, with the uppermost slice corresponding to the highest height reach and the lowermost to the lowest. This multi-layered portrayal enables an unambiguous visual disentanglement between the whole, vertically protracted canopies of vigorous plants and the crumpled, stature-curtailed canopies of lodged plants. Bolstering this spatial view, **Figure 7b** presents the frequency distribution of return tallies spanning the full vertical stature continuum, essentially graphing the number of LiDAR returns at each elevation. A decisive deduction pulled from **Figure 7b** is the surfacing of two distinct apex regions within the return count frequency. The leftward apex is situated at a height of about 0.51 m, whereas the rightward apex is situated at about 2.80 m. These twin apexes are taken to signify a pair of commanding vertical storeys inside the maize canopy. Theoretically speaking, the finest stature cutoff for disjoining lodged from non-lodged segments ought to rest within the hollow domain interposed between these two maxima.

© 2023 The Author(s). | Published by Agro Intelligence Research Press

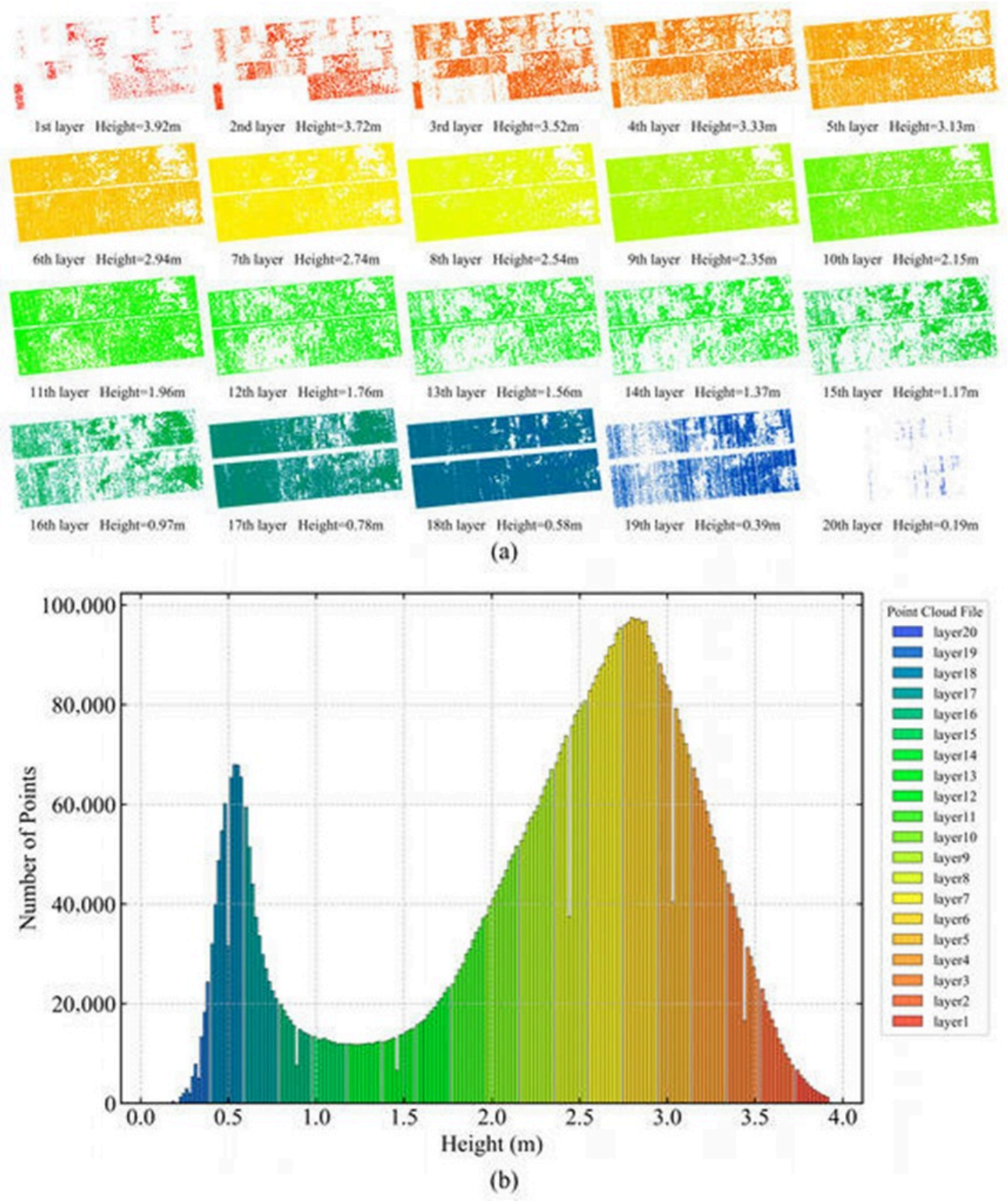

Figure 7. (a) Point cloud layer after height stratification, and (b) Height distribution histogram of all point cloud layers.

To achieve unsupervised, unbiased pinpointing of the stature cutoff for cleaving lodged from non-lodged maize segments, the work at hand innovatively employed a technique that capitalizes on the stepwise layering of point cloud returns, wedded to quantitative benchmarking via the Structural Similarity Index (SSIM) [44, 45]. This modus operandi incorporates a regimented, slice-by-slice heaping of point cloud readings, starting from the loftiest elevation and

© 2023 The Author(s). | Published by Agro Intelligence Research Press

proceeding downward, with each heaped sub-assembly transposed into a binary mask. Those binary masks are then evaluated for structural resemblance against a reference binary mask extracted from the native, unstratified point cloud. The pivotal aim of this undertaking is to identify the vertical cutoff at which the heaped binary mask most faithfully captures the architectural hallmarks of housing discrimination, thereby refining the cutoff specification.

Figure 8a presents a pictorial depiction of a binary mask at a particular waypoint within this stepwise layering regimen, where pale cells indicate the presence of LiDAR returns within the heaped height bands, and dark cells indicate their absence. This representation functions as a freeze-frame of how the spatial footprint of sensed vegetation swells as incrementally shallower height bands are folded in. Augmenting the foregoing, **Figure 8b** illustrates a pair of crucial facets of the breakdown: the blue column diagram renders the SSIM quantity each time a further (lower) point cloud band gets attached to the heap, whereas the red broken trace stands for the tempo of shift in the SSIM quantity linking consecutive heaping stages. As plainly brought out in **Figure 8b**, the SSIM quantity (blue column diagram) obeys a smooth and monotonic climb trajectory as point cloud bands are serially piled from higher toward lower altitudes. This drift is commonsensical, given that each appended band subsumes additional returns from the original cloud, entailing the architectural hallmarks of the heaped binary mask to incrementally home in on those of the original point cloud binary mask. In the closing stage, as all bands stand absorbed, the SSIM value approaches 1, signaling near-perfect architectural concordance.

© 2023 The Author(s). | Published by Agro Intelligence Research Press



(a)

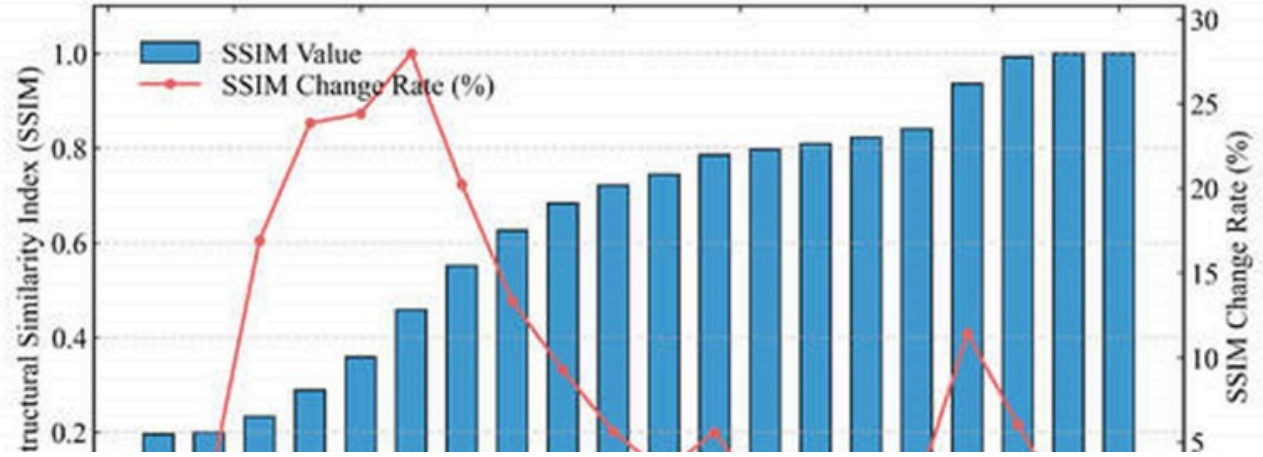

© 2023 The Author(s). | Published by Agro Intelligence Research Press

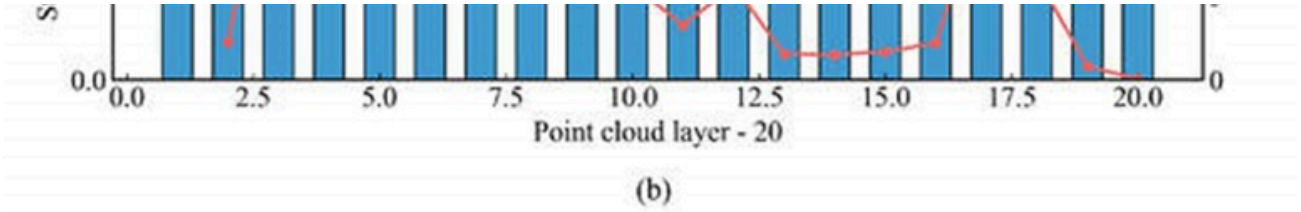

(b)

oscillations arising from inbuilt nonuniformities of maize genotypes, together with stand compactness across the field. Through the inaugural phase of band accumulation (setting forth from the highest returns), such determinants—illustratively genotypic divergences regarding maximum stature or place-specific disparities in plant spacing—present as telling architectural discordances between the heaped (initially exceedingly thin) returns and the unabridged original cloud. This sets off a brisk rise in the SSIM change rate as additional bands (still part of the upper canopy) are ushered in, drawing in a larger fraction of the variability associated with these ingrained field traits. When accumulation proceeds beyond this incipient upper-canopy stage, nonetheless, the incremental admittance of bands commences "thinning down" the comparative contribution of these genotype- and compactness-steered architectural discordances, leading to an attendant drop-off in the change rate. The secondary climax is closely linked to maize lodging. At this juncture in the accumulation course, the height bands being appended correspond to the middle to lower canopy reaches, wherein stature shifts occasioned by lodging become the primary source of architectural dissimilarity, setting the heaped point cloud apart from the original. Toppled specimens having buckled supply returns at these depressed elevations that would be wanting at equivalent compactness in reaches held by sound, erect specimens. In step with accumulation holding on toward steadily depressed elevations, lodging sway remains the prime mover of band architecture within a given critical height window, giving rise to the secondary climax in the SSIM change rate. That said, as the accumulation height draws back further outside this window, the leverage of lodging tapers off (since both sound and lodged specimens may share the same lower architectural constituents), reducing architectural mismatches and causing the change rate to recede yet again. The tertiary climax comes about as the heaped bands close in on the terrain plane. When bands stand amassed to virtually ground-level elevations, their architectural hallmarks align stepwise with the overarching scatter motif of the original point cloud, since near-ground returns are less influenced by canopy undulations and more by the basal ground plane and bottom vegetation. At this point, adventitious perturbations like lodging cease materially shaping band architecture, and the SSIM change rate spikes anew in step with the final lingering architectural minutiae (issued from the bottommost bands) being incorporated. Following this, uninterrupted accumulation yields an exact architectural correspondence between the heaped and original point cloud bands, with the SSIM value approaching 1.

Resting on the all-embracing experimental data appraisal, this enquiry fixed the optimum stature cutoff at 1.76 m, a value matching the elevation of the 12th point cloud band, taken at the secondary climax (lodging-ruled climax) within the SSIM change rate trace. This decisive election rested upon two pivotal reckonings: First off, by the juncture when point clouds had been heaped to the 12th band, the foremost climax (chalked up to genotype and compactness influences) had receded into a sharply etched hollow. This implied that the architectural oscillations arising from nonuniformities in maize genotypes, along with stand compactness, had been in large measure absorbed and their clout had in essence plateaued. Outward from the 12th band, ensuing turnabouts in the point cloud architecture were primarily ascribable to lodging episodes rather than inbuilt field patchiness. In the second place, the breakdown revealed a comparatively torpid tempo of change in SSIM values across the 12th through 16th bands. This leveling off implied that within this circumscribed height band, the perturbations imposed on the point cloud architecture remained stable and exhibited analogous traits across the field. Synthesized, these portents intimated that the sequelae of lodging commenced surfacing prominently outward from the 12th band and emerged as the commanding agency steering point cloud architectural transmutations within the lower bands.

Quantitative assessment of lodging area

To rigorously assess the spatial extent of lodging across the experimental plot, the investigation converted the point cloud archive into an elevation raster grid with a 0.05 m × 0.05 m pixel resolution, thereby preserving intricate spatial textures. Within each grid cell, the mean vertical value of the enclosed point returns was derived, and a partition was executed

© 2023 The Author(s). | Published by Agro Intelligence Research Press

using the best-performing height boundary (1.76 m): cells whose averaged elevation fell shy of this limit were flagged as lodged territory, while those registering above it were assigned to the normally developing class. Such a tactic enables a brisk segregation among disparate growth-state categories. The resulting elevation raster visualization **(Figure 9)** optically demarcates lodged territory (tinted red) from unaffected growing zones (tinted green). By summing the pixel frequencies within the red and green classes, the fractional contribution of lodged terrain relative to the total experimental acreage was resolved. Full computational specifications are collated in **Table 3**. The concluding breakdown reveals that lodged terrain occupies 13.4% of the trial field, providing an easily interpretable numerical indicator of lodging magnitude.

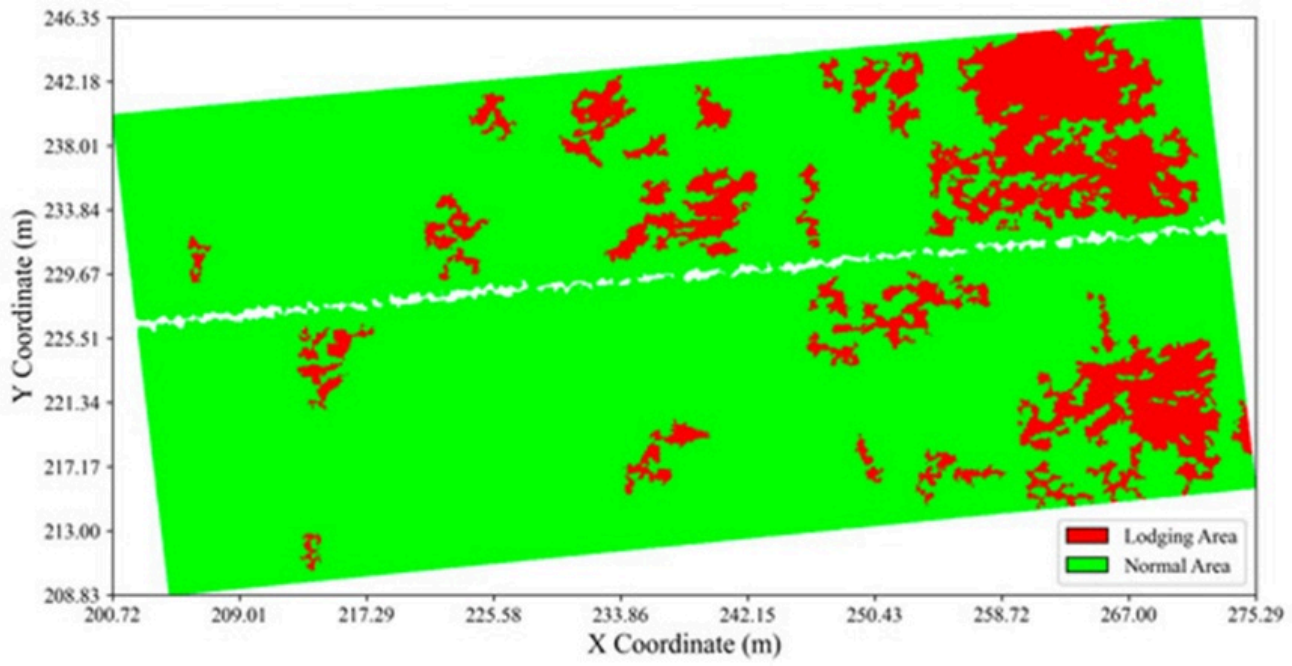

Figure 9. Lodging area prediction based on height raster map.

Table 3. Height raster map conversion parameters.

	Resolution	Red pixels	Total pixels	Height threshold	Proportion of lodging area
Height raster map	0.05 m × 0.05 m	114,760	856,737	1.76 m	13.4%

Height threshold sensitivity analysis

To substantiate the resilience of the height boundary derivation protocol being advocated, the study further performed a boundary perturbation audit. In practical terms, the formerly extracted height limit (1.76 m) was employed as the anchor, and a test window was constructed by appending ±10 cm symmetrically around this anchor (that is, 1.76 m ± 0.1 m). Within this window, 20 candidate height boundaries were positioned at uniform spacing with an incremental step of 1 cm. Based on these 20 candidate values, the point cloud archive covering the study zone was reformulated into equivalent elevation raster grids **(Figure 10)**. To calibrate the effect of height boundary wobble on maize lodging retrieval fidelity, percentage offset was adopted as the evaluative criterion. Taking the 13.4% lodging fraction yielded by the primary experiment as the reference datum, the lodging fraction linked to every candidate boundary and its percentage offset relative to that datum were calculated. The outputs are plotted in **Figure 11**, where the dashed red trace corresponds to the datum with a 10% offset. The study stipulated that a percentage offset below 10% indicates that the shift in the height boundary has no material effect on the appraisal of lodged acreage.

© 2023 The Author(s). | Published by Agro Intelligence Research Press

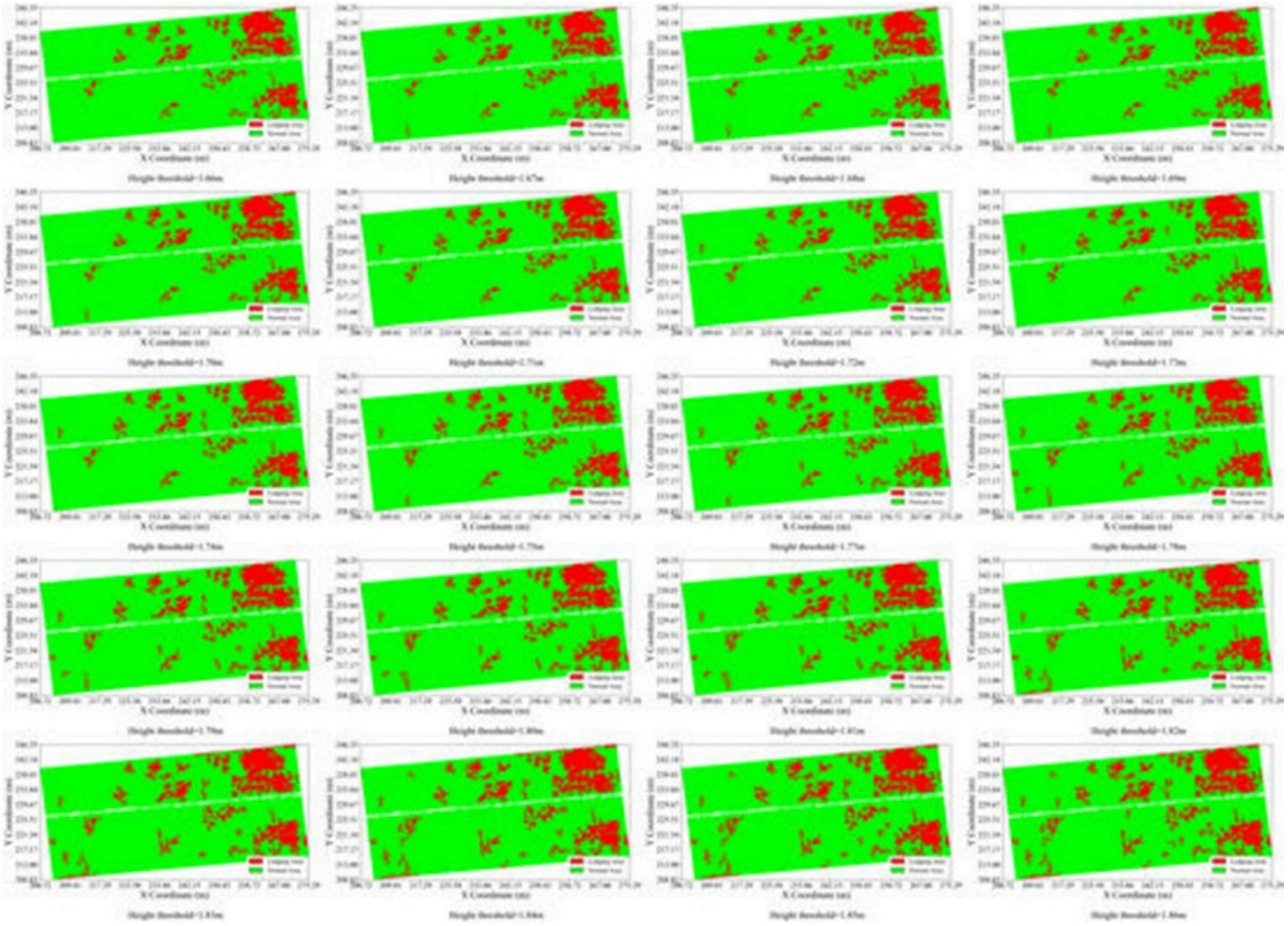

Figure 10. The prediction of the lodging area under different height thresholds.

© 2023 The Author(s). | Published by Agro Intelligence Research Press

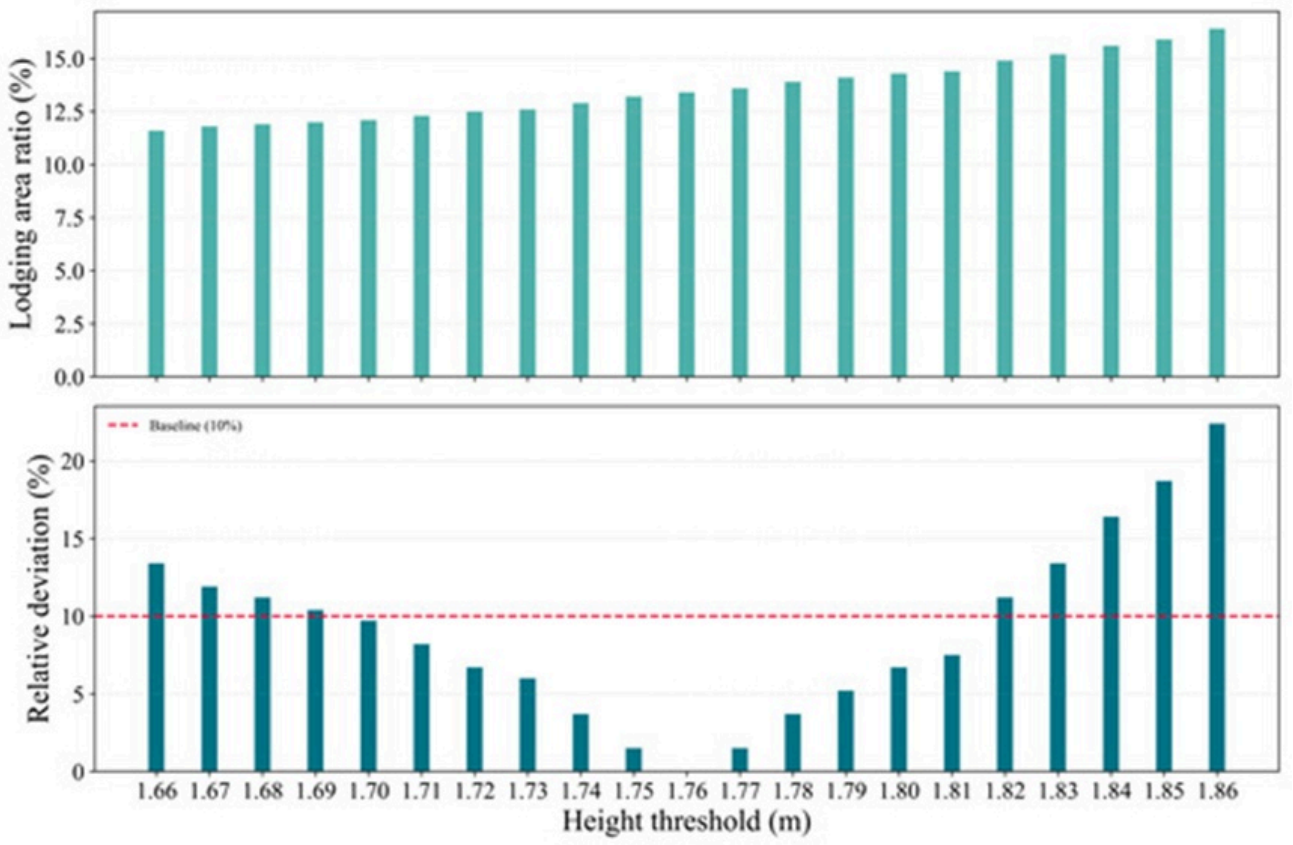

Figure 11. Experimental height threshold: Lodging area ratio and relative deviation.

The experimental outputs indicate that raising the height boundary leads to a steady expansion of the designated lodged zone, a pattern vividly evident in the data scatter shown in the upper panel of **Figure 11**. It follows that the specification of the height boundary materially shapes the determination of lodging acreage, with the soundness of this specification directly dictating the correctness of investigative deductions. More searching scrutiny highlights that, as any given candidate boundary drifts incrementally away from the reference anchor (1.76 m), the corresponding percentage offset in lodging acreage mounts commensurately, as captured by the lower panel data scatter in **Figure 11.** Within the confines of the present inquiry, across the altitude span of 1.70 m to 1.81 m, the percentage offset separating the computed lodging acreage from the reference datum (13.4% lodging fraction) remains beneath the 10% mark. These findings attest that the proposed height boundary strategy retains considerable robustness within a ± 5 cm tolerance band, thereby unequivocally validating the methodological framework described in this work.

Accuracy analysis of the proposed method

Comparison with the accuracy results obtained through manual interpretation

To furnish additional backing for the dependability of the approach introduced in this manuscript, ultra-high-definition RGB photos (boasting an averaged ground sampling distance (GSD) of 7.2 mm) were captured in parallel to function as a decoupled evidentiary stream. The product of expert manual digitization of lodging patches from this photographic record served as the ground reference for fidelity vetting. The digitization workflow was carried out with painstaking care by a trio of specialists possessing deep backgrounds in agricultural remote sensing. To begin with, the ultra-high-definition image data were ingested into ArcGIS Desktop 10.8 (a workstation-grade geospatial information suite engineered by Esri) [46, 47] for spatial analytics and ensuing operations. The interpreters then undertook on-screen tracing at elevated zoom levels, visually spotting and contouring the perimeters of lodged maize sectors, relying on diagnostic markers such as unnatural plant orientation, ruptured canopy texture, and the exposure of the soil substrate. Every specialist operated solo

© 2023 The Author(s). | Published by Agro Intelligence Research Press

to generate an independent version of the lodging map. Afterward, these separate delineations were cross-compared and fused through an agreement-building round to yield a definitive, consolidated ground-reference corpus (as illustrated in **Figure 12**, where blue-filled regions denote the human-digitized lodged sectors), thereby suppressing individual biases and strengthening the authority of the benchmark dataset. Constituting a time-tested and authoritative analytical pathway, this exacting manual digitization produces results of high authority, and its outputs command broad acceptance as a dependable yardstick. By juxtaposing the output of the proposed technique against this solid ground reference, the algorithm's fidelity can be straightforwardly evaluated, and, equally, the likely sources of error, along with their influence intensities, can be uncovered. As shown in **Table 4**, the lodging fraction in the ultra-high-definition RGB imagery, obtained via manual digitization, was 13.1%. In contrast, the lodging fraction estimated by the proposed technique differed from the benchmark by only 2.3%. This 2.3% discrepancy is comparatively subdued compared to parallel investigations in the literature, suggesting that the proposed technique's versatility and stability under complex conditions are consistently maintained.

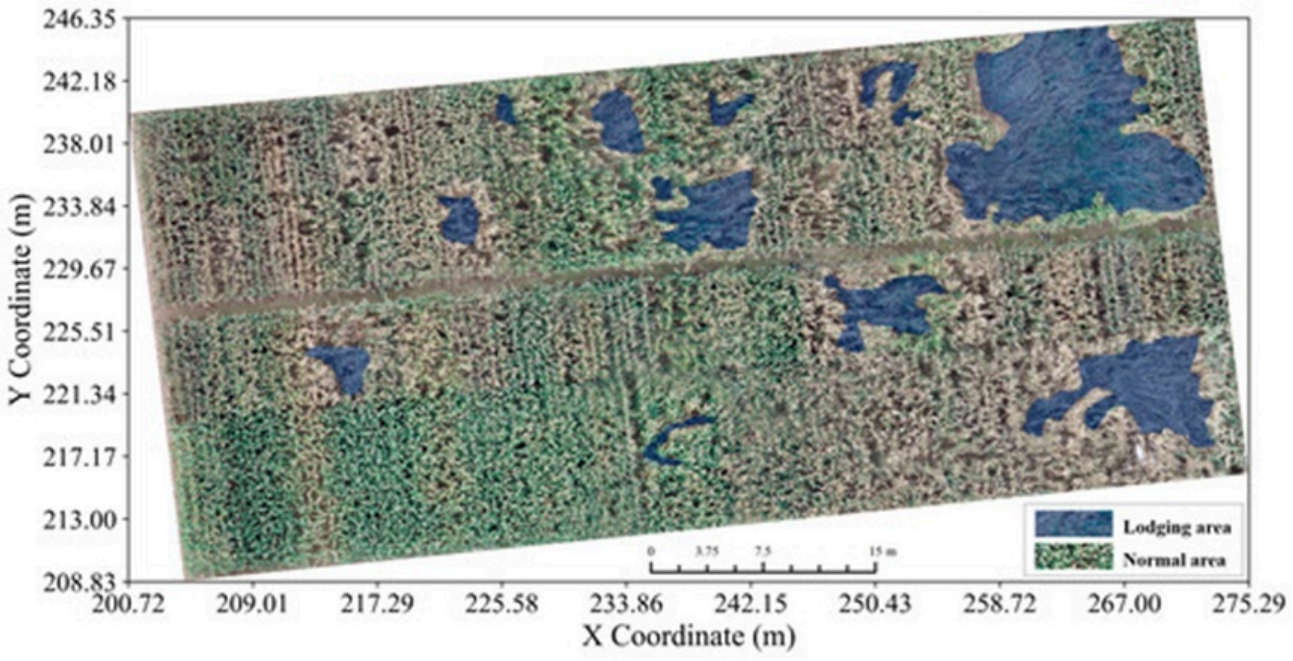

Figure 12. Manual interpretation of the lodging areas from the RGB image.

Table 4. Statistics of lodging results based on RGB images.

	Resolution	Size (pixels)	Red pixels	Total pixels	Proportion of lodging area	Relative deviation[1]	SSIM[2]
RGB image	7.2 mm GSD	2942 × 1485	432,642	3,303,990	13.1%	2.3%	0.95

[1]: The relative deviation between the lodging area of 13.4% calculated at a height threshold of 1.76 m and the lodging area of 13.1% obtained by manual interpretation. [2]: The structural similarity between the lodging area map predicted based on the height threshold of 1.76 m and the lodging area map obtained by manual interpretation.

The research documented in this paper goes a step further by recasting manual digitization outputs derived from ultra-high-definition RGB imagery into polygon representations and superimposing them with the raster depiction of lodging sectors delimited by the height boundary proposed in this work. As shown in **Figure 13**, the lodging sectors isolated by the two pathways exhibit substantial spatial co-registration, with a computed Structural Similarity Index (SSIM) of 0.95

© 2023 The Author(s). | Published by Agro Intelligence Research Press

between the paired representations—an extraordinarily high value. This outcome points powerfully toward close concordance between the height-boundary-grounded routine for pinpointing lodging sectors and the manual digitization findings, thereby bearing out the utility and accuracy of the proposed investigative design. At the same time, by probing the blue-matched zones outlined in **Figure 13b**, a set of crucial observations emerged. First, the height-boundary-grounded extraction routine faces fundamental constraints in thinly populated planting zones. Owing to the more expansive areas of bare-earth visibility and sparser point cloud coverage within such zones, denuded soil stands at an elevated risk of erroneous classification as lodging, leading to inaccuracies in extraction products. Secondly, RGB-dependent manual digitization is inherently susceptible to subjective judgment. Especially within tangled field backdrops, lodging sectors often assume jagged outlines, and the frontiers marking the transition from mature-stage lodging to ordinarily developing maize can remain ambiguous. This haziness not only compounds the challenge of manual digitization but may also provoke significant inter-interpretational inconsistency. Forthcoming investigations might aim to combine these dual remote sensing technologies to offset their respective shortcomings.

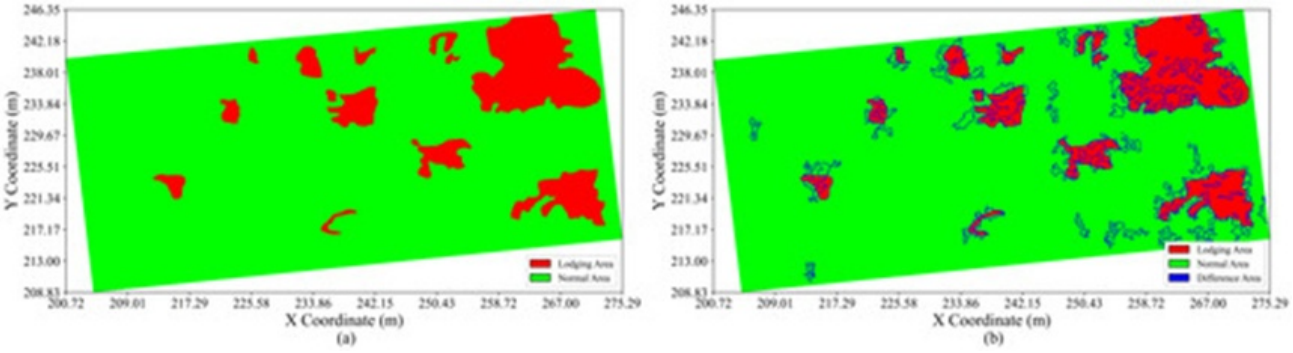

Figure 13. (a) Raster map based on RGB image conversion, and (b) Differential regions with blue highlights.

Comparison and analysis with the classic threshold selection schemes

As an essential conduit of three-dimensional spatial intelligence, the elevation attributes of point cloud records can be conceptualized as a variant of "single-band grayscale waveform." This conceptual linkage aligns closely with the construct of grayscale intensities in image manipulation, in which the frequency distribution of elevation magnitudes is directly visualized via an elevation histogram. In particular, substantial differences in elevation distributions commonly separate lodged from unaffected territory. For example, lodged patches tend to register depressed elevation magnitudes, whereas unaffected patches tend to display elevated ones. This dichotomy presents as a clear-cut "bimodal pattern" in the elevation histogram, with the paired modes aligning with the elevation distributions of lodged and unaffected territory. By harnessing this bimodal distributional property, self-tuning height boundary identification can be achieved using traditional data-driven methods. Among such methods, Otsu's Method has become a frequently selected option thanks to its simplicity, operational speed, and aptitude for bimodal distributions [48-50]. To compare the self-tuning boundary selection scheme advanced in the present study with conventional boundary-picking strategies, further tests were run using Otsu's Method for height boundary determination, with the outputs shown in **Figure 14**.

© 2023 The Author(s). | Published by Agro Intelligence Research Press

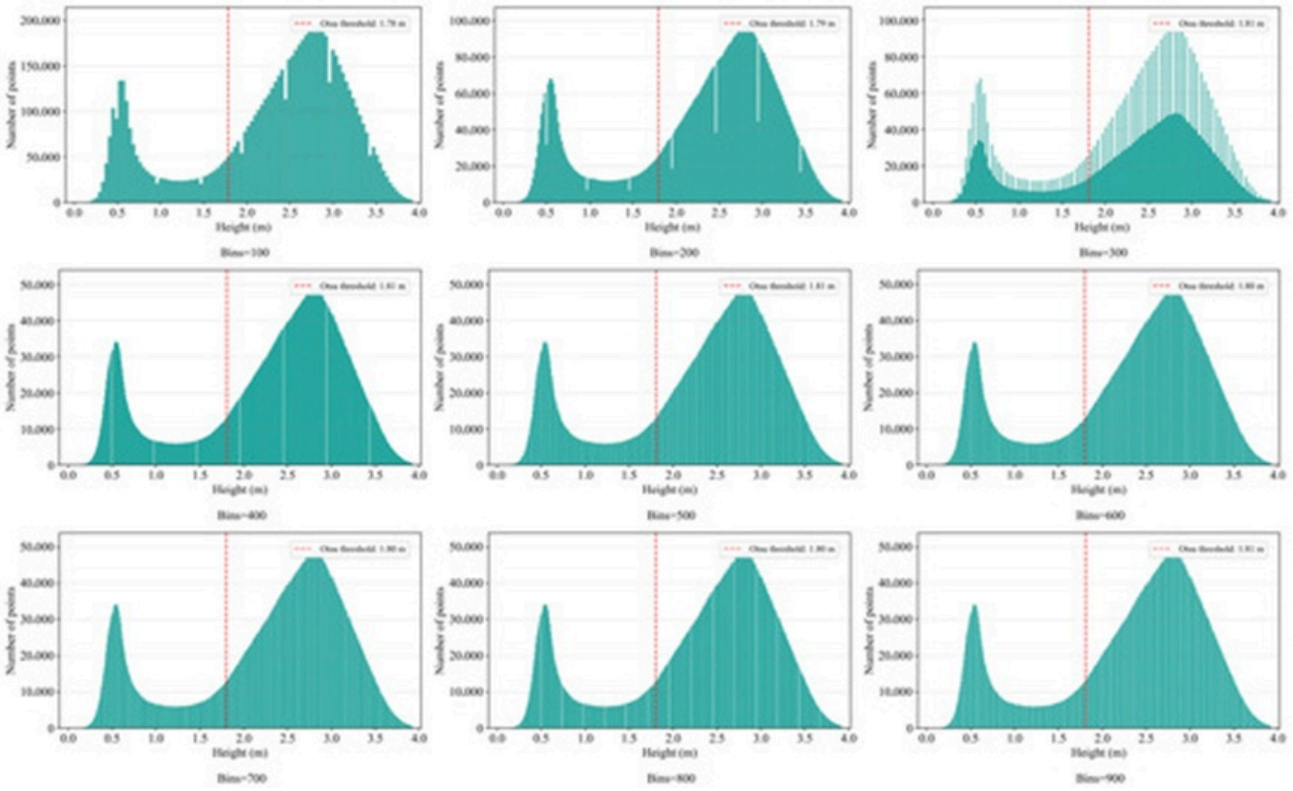

Figure 14. Otsu's Method: height threshold selection under different parameter settings.

The experimental data indicate that boundary picking via Otsu's method is highly sensitive to parameter settings. When the point cloud histogram is segmented into variable bin counts, the resulting height boundaries exhibit erratic oscillations, making it less straightforward to isolate a single, steady boundary for analytical applications. To gauge the accuracy of lodging acreage projections, a side-by-side comparison was conducted between the proposed technique and Otsu's method under various boundary conditions **(Figure 15)**. The data show that the offsets in the projected lodging acreage fraction using Otsu's method across varying boundaries exceed those obtained with the proposed technique, which yields an offset of merely 2.3% compared to the manual-digitized benchmark values. This insight further supports the resilience and correctness of the proposed technique.

© 2023 The Author(s). | Published by Agro Intelligence Research Press

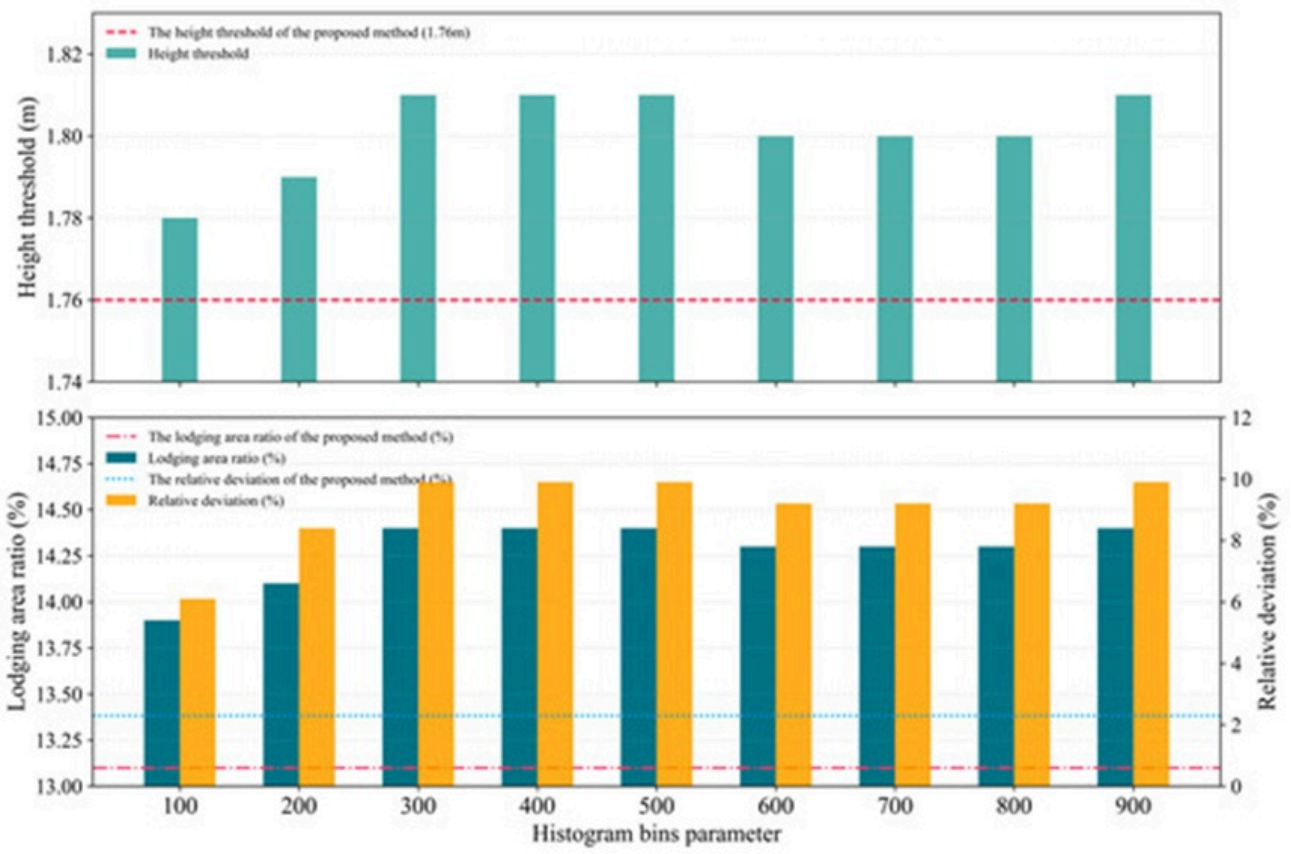

Figure 15. Comparison of height threshold determination and lodging prediction performance: Otsu's method vs. proposed method.

It is worth noting that, in essence, all data-driven self-tuning boundary selection frameworks remain susceptible to parametric influence. Curtailing the scope of such influence stands as an indispensable and inescapable challenge confronting any research agenda. While the self-tuning height boundary selection framework introduced in this inquiry is affected to some degree by point cloud stratification parameters, this topic will receive exhaustive treatment in the chapters that follow. Preliminary results suggest that when the stratification parameters are set to even multiples of 10, the proposed framework can unambiguously converge to an optimal boundary, thereby alleviating the instability in boundary selection associated with parametric sensitivity in Otsu's method.

The influence of point cloud layering parameters on the accuracy results

Within the proposed scheme advanced in this study, determining the number of point cloud slicing levels is critical to obtaining reliable height boundaries. Extending on the foregoing work that anchored the slicing level count at 20, this paper conducts a suite of controlled experiments to investigate whether appreciable divergences arise in the height boundaries derived from SSIM analysis across variable slicing level configurations. The experiments operate with ten distinct level counts spanning from 10 to 100 (specifically, 10, 20, 30, 40, 50, 60, 70, 80, 90, 100) and produce the associated SSIM variation traces in adherence to the established research protocol **(Figure 16)**, from which the best-performing height boundaries per level arrangement are subsequently extracted **(Figure 17)**. Empirical findings reveal that whenever the count of slicing levels constitutes an even multiple of 10 (e.g., 20, 40, 60, 80, 100), the height boundary consistently locks onto 1.76 m, an outcome indicative of robust convergence of point cloud slicing toward a stationary boundary under these particular level specifications, thereby safeguarding the trustworthiness of results. Contrariwise, when the level count corresponds to an odd multiple of 10 (e.g., 10, 30, 50, 70, 90), the height boundary displays marked instability, manifesting specifically as a gradual upward drift commensurate with increasing level count: the boundary

© 2023 The Author(s). | Published by Agro Intelligence Research Press

plunges to a floor of 1.17 m at 10 levels and edges toward the steady even-multiple value (1.76 m), cresting at 1.74 m under 90 levels. This divergence plausibly originates from the even partitioning of point cloud data across the slice stack. More precisely, setting height boundaries at multiples of 10 (even quantities) promotes a more balanced distribution of data mass across slices, thereby lessening information loss or surplus induced by an inadequately sized slice stack.

In contrast, adopting odd multiples of 10 as boundaries tends to disturb this balance, often leading to lopsided data volume partitioning across slices during stratification and, consequently, a slight boundary drift. Furthermore, as the slice count increases, the slicing process asymptotically approaches a “limit regime,” pushing the height boundary toward stabilization—a tendency suggesting that point cloud slicing technology can effectively encapsulate core data signatures and reduce inaccuracies caused by suboptimal slice count selection when a sufficiently fine slicing granularity is used. Through a structured exploration of the interplay between slice count and height boundary, the present study verifies that even multiples of slices (most especially 20 slices) strike the best equilibrium between throughput and accuracy, vindicating the scientific basis and efficiency of the previously codified 20-slice configuration and consequently negating the need for substantial revision of the established protocol.

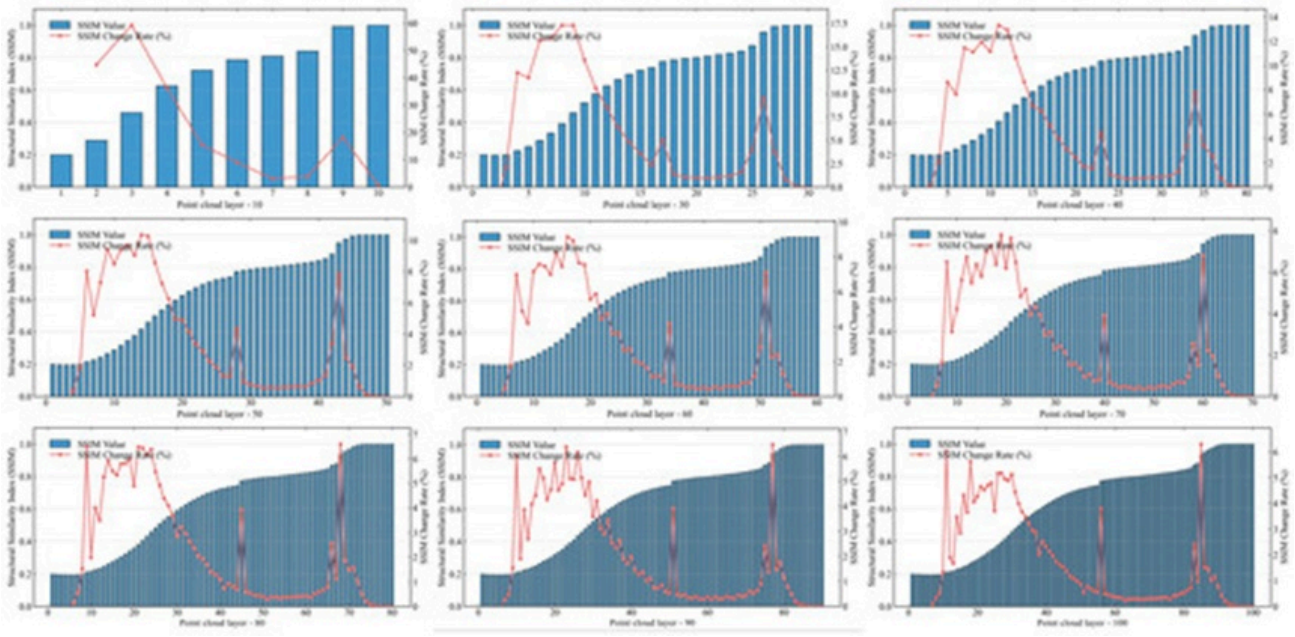

Figure 16. Statistics of SSIM changes under different numbers of point cloud layers.

© 2023 The Author(s). | Published by Agro Intelligence Research Press

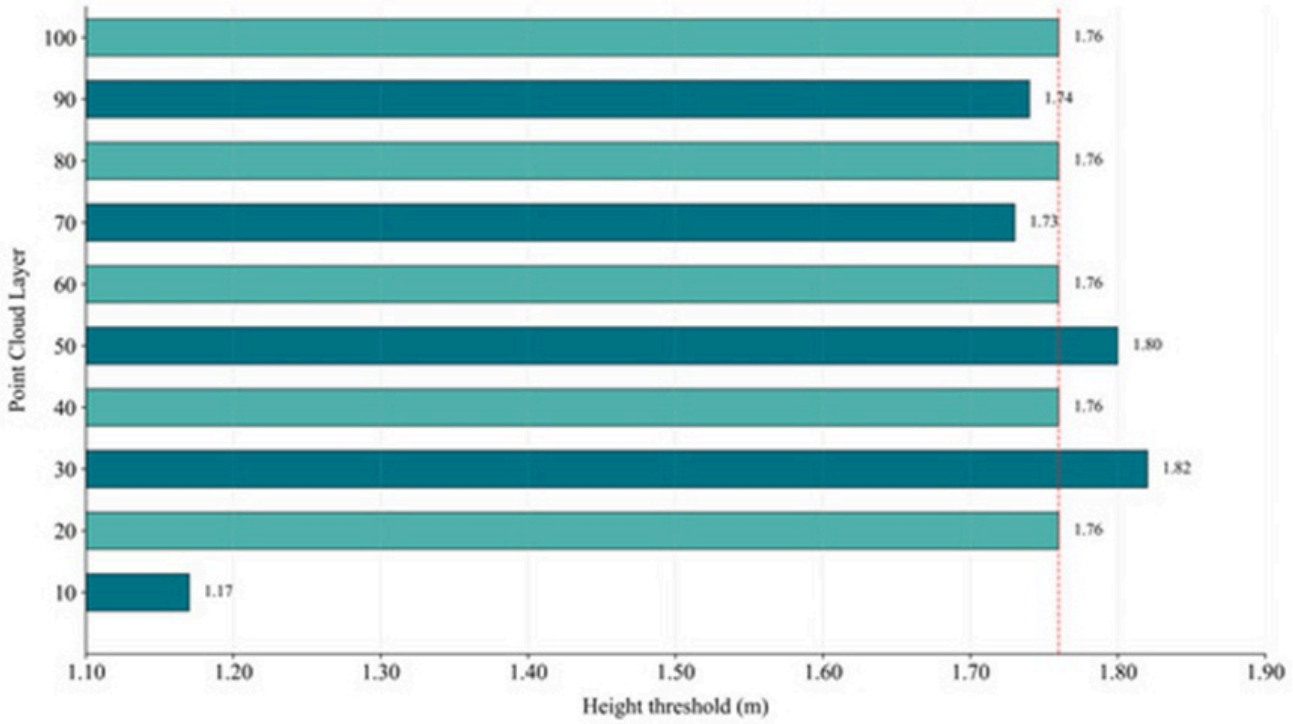

Figure 17. Optimal height threshold bar chart statistics.

The effect of UAV flight altitude on lodging monitoring using point cloud data

Research on the accuracy of height threshold monitoring under low spatial resolution

Fluctuations in the operational ceiling of an unmanned aerial vehicle (UAV) tangibly modulate the richness of point cloud captures [51-53]. To gauge the extent to which point cloud richness moderates the precision of the investigative framework set out herein, a coupling study was conducted in which UAV operational ceilings were systematically varied across flight missions. The structural likeness scoring run on the binary masks generated by point cloud sectioning revealed a drastic reconfiguration in the silhouette of the structural likeness variation rate locus. Parting ways with foregoing runs, which customarily surfaced three crisply delineated apices, the present experimental round yielded only two apices. This dyad of apices maps, respectively, onto the accelerated convergence of architectural divergences rooted in varietal identity and stand compactness, and the accelerated convergence of divergences born from lodging. The lacuna left by the diagnostic inflection that earlier runs had linked to incipient elevation discrepancies tied to lodging—namely, the second apex along the SSIM variation rate locus—deprived the analysis of a dependable navigational mark for homing in on a serviceable height cutoff. As a direct outgrowth, precisely delimitating the elevation band within which lodging exerts its influence became a formidable undertaking. While tuning knobs for point cloud sectioning granularity were adjusted to refine output quality (as schematically shown in **Figure 18**), the overall architecture of the structural likeness variation rate locus proved largely impervious to such adjustments. This signals that the foundational shortcoming of the algorithmic pipeline does not reside in parameter settings; rather, point cloud richness exerts an overriding influence on the monitoring readouts. Reformulated another way, the fidelity that the structural likeness assay can deliver is inescapably tethered to the intrinsic caliber of the point cloud feed. Further, the study shows that the chosen operational ceiling of the UAV leaves a deep imprint on the sensor's ability to resolve fine-grained undulations in canopy elevation. Under more elevated flight ceilings, the resultant point cloud gravitates toward diffuseness, undercutting its potency to faithfully mirror the crop's vertical architecture. At the antipode, depressed flight ceilings generate tightly packed point ensembles that are far more adept at conserving the delicate elevation variation markers nestled within the

© 2023 The Author(s). | Published by Agro Intelligence Research Press

maize canopy. Accordingly, the pipeline championed in the present work is best suited for surveillance contexts with modest operational ceilings (e.g., 25 m), where it can deliver a high-fidelity assessment of lodging status.

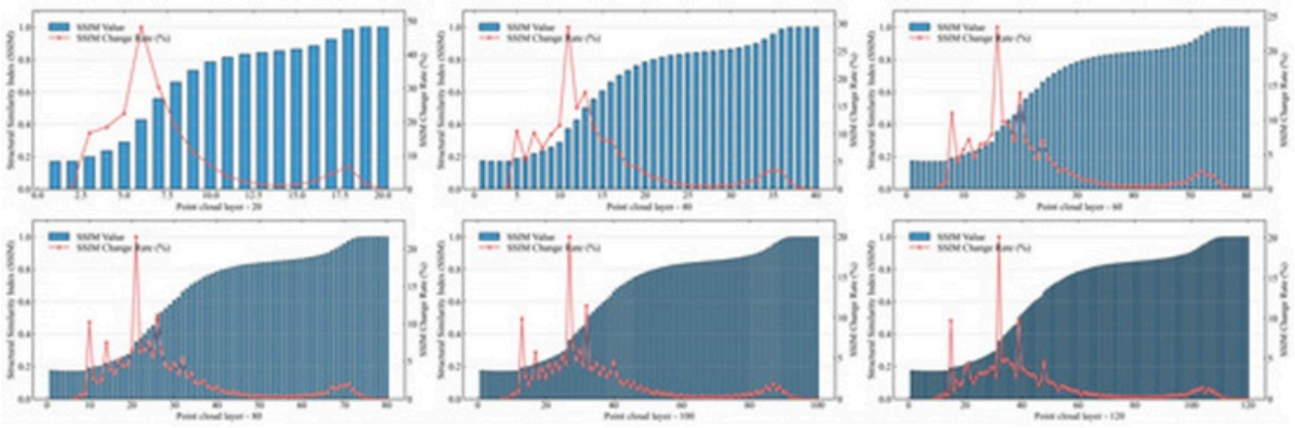

Figure 18. Statistics of structural similarity after different point cloud layering parameters at a flight altitude of 80 m.

Research on the transferability of height threshold under low-altitude flight pre-training

The fact that low-ceiling UAV traverses supply data of premium richness is counterbalanced by the reality that their constrained areal footprint often undercuts the economy of surveillance operations. To palliate this tension, the present effort undertook a scoping inquiry into whether a height boundary mined from low-ceiling traverse data could be fruitfully exported to high-ceiling observational regimes. Within the experimental matrix, the height boundary of 1.76 m—extracted during traverses pegged at a 25 m operational ceiling—was applied unmediated to flag lodged maize individuals from data gathered at an 80 m ceiling. The collateral computational specifications are assembled in **Table 5**, with the predictive renditions portrayed in **Figure 19**. As inspection of this figure makes plain, the algorithmically projected lodging footprint registers a pronounced degree of concurrence with the footprints derived via human digitization. Drawing upon the tallies in **Table 5**, the lodging area fraction determined through this transpositional route was 13.8%, a figure that differs from the hand-digitized datum of 13.1% by only 5.3%. Such an upshot suggests that, to a meaningful degree, the boundary value possesses an aptitude for cross-ceiling porting and can reliably underpin monitoring exercises conducted beneath elevated flight ceilings. While recognizing that the empirical scope of this inquiry remained circumscribed, the evidence provisionally supports the contention that low-ceiling LiDAR-derived height boundaries exhibit meaningful resilience when applied to high-ceiling traverse data. This materializes as a demonstration of the methodology's transplantability, thereby amplifying the operational latitude of UAV-LiDAR toolsets across the agricultural management spectrum.

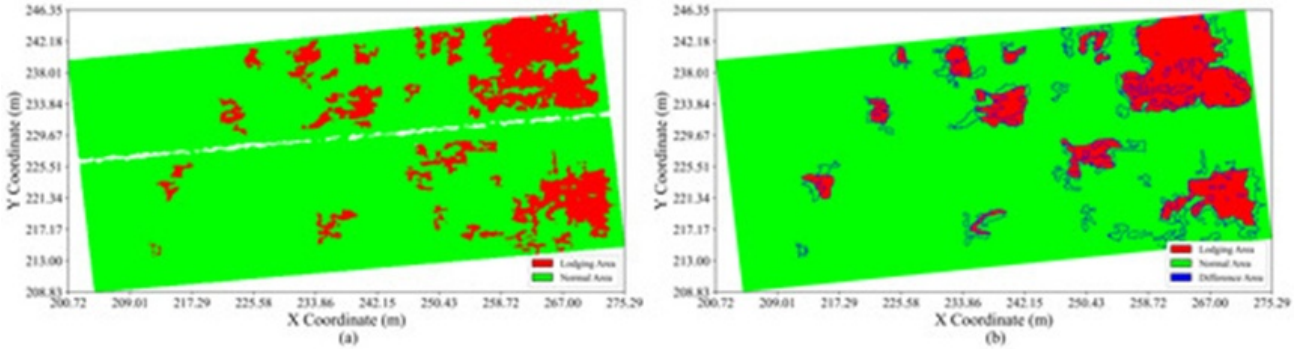

Figure 19. (a) Prediction of the lodging area based on the height threshold of 1.76 m at a flight altitude of 80 m, and (b) Comparison between the experimental prediction results and the results of manual interpretation.

Table 5. Height raster map conversion parameters at a flight altitude of 80 m.

© 2023 The Author(s). | Published by Agro Intelligence Research Press

	Resolution	Size (pixels)	Red pixels	Total pixels	Height threshold	Proportion of lodging area	Relative deviation[1]	SSIM[2]
Height raster map	0.1 m × 0.1 m	737 × 367	29,215	212,229	1.76 m	13.8%	5.3%	0.95

[1]: Calculate the relative deviation between the calculated lodging area percentage of 13.8% and the manually interpreted result of 13.1%, and [2]: The structural similarity between the lodging area map predicted based on the height threshold of 1.76 m and the lodging area map obtained by manual interpretation.

Limitations and future directions of this research

Spanning the patchwork of smallholder farming practices that blanket rural China, the hegemonic cultivation templates embrace block-partitioned seeding, polyvarietal intercropping, and multi-density stand layouts. These byzantine agronomic schemes stand in pointed contradistinction to the streamlined logic of industrialized broad-acre monocropping, and they conjure a distinctive suite of techno-operational obstacles—chief among them the detection and quantification of crop lodging. Off-the-shelf per-pixel taxonomical classifiers regularly break down when thrust into such heterogeneous tableaux, not least because of the prohibitive expense attached to the curation of annotated learning exemplars. The present work mounts a rejoinder to this impasse by proposing a crop lodging detection framework grounded in a self-adjusting height threshold. Its cardinal virtue resides in the capacity to carry out expeditious lodging flagging coupled with numeric areal estimation inside fragmentary parcels governed by elaborate planting geometries. This design philosophy concurrently reduces the reliance on human-supplied annotations while delivering a lean yet high-impact technical solution purpose-built for the realities of rural Chinese agriculture.

While the self-adjusting height demarcation selection procedure described in these pages shows appreciable traction under bench-test conditions, it nonetheless operates within recognized current strictures. In the first instance, the empirical evidence base was drawn from a numerically modest ensemble of field sites. This circumstance inevitably constrains the extrapolability and evidentiary weight of the deductions. To strengthen the claims regarding the protocol's potency and ruggedness, forthcoming research iterations should systematically broaden the evidential foundation by integrating larger and more ecologically diverse data corpora. In the second instance, the terrain underlying the experimental precinct was comparatively planar, a felicitous condition that permitted sidestepping the need for elaborate height rectification procedures to dampen topographic artifacts during point cloud preprocessing. While this shortcut trims the computational tax, it effectively shears the protocol's remit, confining its demonstrated reliability principally to flat-earth deployment scenarios. For topographies characterized by emphatic relief (e.g., rolling uplands or steep inclines), the scheme in its current incarnation would likely struggle to faithfully lock onto the target signal. Research vectors moving forward should bake in off-the-shelf terrain normalization toolchains to mitigate the complications posed by morphologically complex land surfaces. As one concrete pathway, terrain-induced corruptions could be systematically stripped away via proprietary software suites or community-curated, open-licensed Python (v3.6+) scripting (e.g., https://github.com/lloydwindrim/forest_3d_app/blob/master/src/forest3D/ground_removal.py (accessed on 30 October 2025)), moves that would jointly enhance the framework's morphological pliability.

Conclusion

The height-bounded detection paradigm provides a means for swift localization of maize lodging within tangled field tableaux (e.g., multi-cultivar intercropping matrices). The manuscript at hand provides an exhaustive dissection of an unattended height boundary derivation technology, aiming to deliver accurate maize lodging intelligence across cultivation landscapes marked by a rich mosaic of varieties and population densities. The empirical harvest attests that, by braiding together height-resolved slicing with structural likeness quantification within a field-scale maize point cloud processing workflow, the proposed methodology effectively captures both the upright and lateral canopy architectural dislocations induced by lodging and accurately pinpoints a height boundary. By brandishing this boundary, lodging-affected patches are demarcated through a height-conditioned false-color rendering of the point ensemble and subsequently reprojected

© 2023 The Author(s). | Published by Agro Intelligence Research Press

into a gridded elevation map. This transformation paves the way for the numerical mensuration of lodging extent. Experimental substantiation reveals that the discrepancy between the tracking exactitude of the proposed framework (13.4%) and the output of manual digitization (13.1%) narrows to a slender 2.3%. Supplementing this, a robustness audit of the height boundary confirms that when this parameter is perturbed within a ±5 cm corridor, the resultant percentage offset in lodging acreage mensuration stays firmly beneath the 10% ceiling—a finding that certifies, in full, the trustworthiness and operational ruggedness of the propounded framework. As a closing synthesis, the height-boundary-driven automated tracking technology crystallized through this body of work furnishes an unprecedented technical response to the challenge of maize lodging flagging in structurally complex field settings, while, in parallel, highlighting the deployment promise and novel value of UAV-mounted LiDAR systems within the precision agriculture arena.

Acknowledgements

None

Conflict of interest

None

Financial support

This research was funded by the National Natural Science Foundation of China (NSFC), grant number 61972363; the Central Government Leading Local Science and Technology Development Fund Project, grant number YDZJSX2021C008; and the Fundamental Research Program of Shanxi Province, grant number 202203021221104.

Ethics statement

None

Received: 17 Apr 2022 Revised: 22 Jun 2022 Accepted: 08 Jul 2022
Published online: 25 May 2023

Rights and permissions

Open Access The author(s) retain copyright. This article is licensed under the Creative Commons Attribution-NonCommercial-ShareAlike 4.0 International License. It may be shared and adapted for non-commercial purposes with appropriate attribution, an indication of changes, and distribution of adaptations under the same license. Third-party material may be subject to separate terms identified in its credit line. View the license at https://creativecommons.org/licenses/by-nc-sa/4.0/.

References

1. Wei X, Zhang J, Wang D, Zhao C, Guga S, Guo Y, et al. Comprehensive risk fine dynamic assessment and zoning of maize high wind lodging disasters in Jilin Province, China. Eur J Agron. 2025;170:127710.

2. Liu Y, Nie C, Zhang Z, Wang Z, Ming B, Xue J, et al. Evaluating how lodging affects maize yield estimation based on UAV observations. Front Plant Sci. 2023;13:979103.

3. Zhang P, Gu SC, Wang YY, Xu CC, Zhao YT, Liu XL, et al. The relationships between maize (Zea mays L.) lodging resistance and yield formation depend on dry matter allocation to ear and stem. Crop J. 2023;11:258–68.

4. Mu HM, Wang ZZ, Sun LF, Huang Y, Song YF, Zhang R, et al. Optimizing nitrogen fertilization and planting density management enhances lodging resistance and wheat yield by promoting carbohydrate accumulation and single spike development. Crop Sci. 2024;64:3461–79.

5. Ahmad I, Batyrbek M, Ikram K, Ahmad S, Kamran M, Misbah, et al. Nitrogen management improves lodging resistance and production in maize (Zea mays L.) at a high plant density. J Integr Agric. 2023;22:417–33.

6. Yang J, Meng X, Yang S, Yang J, Li Z, Yang Q, et al. A simple method for lodging resistance evaluation of maize in the field. Front Plant Sci. 2023;13:1087652.

7. Zhang Q, Zhang GL, Zhang Y, Xiao XM, You NS, Li ZC, et al. Coupling GEDI LiDAR and Optical Satellite for Revealing Large-Scale Maize Lodging in Northeast China. Earths Future. 2024;12:e2023EF003590.

8. Kumar M, Bhattacharya BK, Pandya MR, Handique BK. Machine learning based plot level rice lodging assessment using multispectral UAV remote sensing. Comput Electron Agric. 2024;219:108754.

9. Feng GQ, Wang C, Wang AC, Gao YY, Zhou YA, Huang S, et al. Segmentation of Wheat Lodging Areas from UAV Imagery Using an Ultra-Lightweight Network. Agriculture. 2024;14:244.

10. Chauhan S, Darvishzadeh R, Boschetti M, Pepe M, Nelson A. Remote sensing-based crop lodging assessment: Current status and perspectives. ISPRS J Photogramm Remote Sens. 2019;151:124–40.

11. Yan Y, Song F, Sun J. The application of UAV technology in maize crop protection strategies: A review. Comput Electron Agric. 2025;237:110679.

12. Shu MY, Bai K, Meng L, Yang XH, Li BG, Ma YT. Assessing maize lodging severity using multitemporal UAV-based digital images. Eur J Agron. 2023;144:126754.

13. Sun Q, Chen L, Xu X, Gu X, Hu X, Yang F, et al. A new comprehensive index for monitoring maize lodging severity using UAV-based multispectral imagery. Comput Electron Agric. 2022;202:107362.

14. Liu T, Zhu S, Yang T, Zhang W, Xu Y, Zhou K, et al. Maize height estimation using combined unmanned aerial vehicle oblique photography and LIDAR canopy dynamic characteristics. Comput Electron Agric. 2024;218:108685.

15. Lei L, Li Z, Yang G, Yang H. High-Throughput Extraction of the Distributions of Leaf Base and Inclination Angles of Maize in the Field. IEEE Trans Geosci Remote Sens. 2023;61:4411228.

16. Gao M, Yang F, Wei H, Liu X. Individual Maize Location and Height Estimation in Field from UAV-Borne LiDAR and RGB Images. Remote Sens. 2022;14:2292.

17. Zhang Z, Flores P, Igathinathane C, Naik DL, Kiran R, Ransom JK. Wheat Lodging Detection from UAS Imagery Using Machine Learning Algorithms. Remote Sens. 2020;12:1838.

18. Li G, Han W, Huang S, Ma W, Ma Q, Cui X. Extraction of Sunflower Lodging Information Based on UAV Multispectral Remote Sensing and Deep Learning. Remote Sens. 2021;13:2721.

19. Guan H, Liu H, Meng X, Luo C, Bao Y, Ma Y, et al. A quantitative monitoring method for determining maize lodging in different growth stages. Remote Sens. 2020;12:3149.

20. Sun Q, Sun L, Shu M, Gu X, Yang G, Zhou L. Monitoring maize lodging grades via unmanned aerial vehicle multispectral image. Plant Phenomics. 2019;2019:5704154.

© 2023 The Author(s). | Published by Agro Intelligence Research Press

21. Zhu Q, Wang K, Liang D, Tang J. WLUSNet: A lightweight wheat lodging segmentation network based on UAV image. Comput Electron Agric. 2025;237:110587.

22. Wang D, Zhao M, Li Z, Xu S, Wu X, Ma X, et al. A survey of unmanned aerial vehicles and deep learning in precision agriculture. Eur J Agron. 2025;164:127477.

23. Cao W, Qiao Z, Gao Z, Lu S, Tian F. Use of unmanned aerial vehicle imagery and a hybrid algorithm combining a watershed algorithm and adaptive threshold segmentation to extract wheat lodging. Phys Chem Earth Parts A/B/C. 2021;123:103016.

24. Jin S, Su Y, Gao S, Wu F, Hu T, Liu J, et al. Deep learning: Individual maize segmentation from terrestrial lidar data using faster R-CNN and regional growth algorithms. Front Plant Sci. 2018;9:866.

25. Miao L, Wang XY, Yu C, Ye CY, Yan YY, Wang HS. What factors control plant height?. J Integr Agric. 2024;23:1803–24.

26. Zhao JH, Chen SD, Zhou B, He HX, Zhao YJ, Wang Y, et al. Multitemporal field-based maize plant height information extraction and verification using solid-state lidar. Agriculture. 2024;14:1069.

27. Jayasuriya N, Guo Y, Hu W, Ghannoum O. Machine vision based plant height estimation for protected crop facilities. Comput Electron Agric. 2024;218:108669.

28. Long J, Zhang Z, Zhang Q, Zhao X, Igathinathane C, Xing J, et al. Comprehensive wheat lodging detection under different UAV heights using machine/deep learning models. Comput Electron Agric. 2025;231:109972.

29. Cai C, Zhao H, Zhang H, Wang C, Wang Z, Liu M, et al. Timely assessment of maize lodging severity with limited samples using multi-temporal Sentinel-1 and Sentinel-2 data across large spatial extents. Comput Electron Agric. 2025;237:110671.

30. Wang C, Xu S, Yang C, You Y, Zhang J, Kuai J, et al. Determining rapeseed lodging angles and types for lodging phenotyping using morphological traits derived from UAV images. Eur J Agron. 2024;155:127104.

31. Ren Z, Zheng H, Chen J, Chen T, Xie P, Xu Y, et al. Integrating UAV, UGV and UAV-UGV collaboration in future industrialized agriculture: Analysis, opportunities and challenges. Comput Electron Agric. 2024;227:109631.

32. Wilke N, Siegmann B, Klingbeil L, Burkart A, Kraska T, Muller O, et al. Quantifying lodging percentage and lodging severity using a uav-based canopy height model combined with an objective threshold approach. Remote Sens. 2019;11:515.

33. Mengistie E, McDonald AG. Effect of cell wall compositions on lodging resistance of cereal crops: Review. J Agric Sci. 2023;161:794–807.

34. Madec S, Baret F, de Solan B, Thomas S, Dutartre D, Jezequel S, et al. High-Throughput Phenotyping of Plant Height: Comparing Unmanned Aerial Vehicles and Ground LiDAR Estimates. Front Plant Sci. 2017;8:2002.

35. Malambo L, Popescu SC, Murray SC, Putman E, Pugh NA, Horne DW, et al. Multitemporal field-based plant height estimation using 3D point clouds generated from small unmanned aerial systems high-resolution imagery. Int J Appl Earth Obs Geoinf. 2018;64:31–42.

36. Zhou L, Gu X, Cheng S, Yang G, Shu M, Sun Q. Analysis of Plant Height Changes of Lodged Maize Using UAV-LiDAR Data. Agriculture. 2020;10:146.

37. Chu TX, Starek MJ, Brewer MJ, Murray SC, Pruter LS. Assessing Lodging Severity over an Experimental Maize (Zea mays L.) Field Using UAS Images. Remote Sens. 2017;9:923.

38. Hu XQ, Gu XH, Sun Q, Yang Y, Qu XZ, Yang X, et al. Comparison of the performance of Multi-source Three-dimensional structural data in the application of monitoring maize lodging. Comput Electron Agric. 2023;208:107782.

© 2023 The Author(s). | Published by Agro Intelligence Research Press

39. Wang M, Sun Q, Che XH, Chen L, Cui YP, Liu J, et al. Mapping rice lodging severity using dual-pol Sentinel-1 SAR data: Polarimetric parameters, lodging sensitivity, and fuzzy classification modelling. Int J Remote Sens. 2025;46:2748–66.

40. Huang X, Xuan F, Dong Y, Su W, Wang X, Huang J, et al. Identifying corn lodging in the mature period using chinese gf-1 pms images. Remote Sens. 2023;15:894.

41. Yin DM, Wang L, Lu Y, Shi C. Mangrove tree height growth monitoring from multi-temporal UAV-LiDAR. Remote Sens Environ. 2024;303:114002.

42. Ma X, Wei B, Guan H, Yu S. A method of calculating phenotypic traits for soybean canopies based on three-dimensional point cloud. Ecol Inform. 2022;68:101524.

43. Wang DS, Zhao MH, Li ZL, Wu XH, Li N, Li DC, et al. Classification of maize lodging types using UAV-SAR remote sensing data and machine learning methods. Comput Electron Agric. 2024;227:109637.

44. Bakurov I, Buzzelli M, Schettini R, Castelli M, Vanneschi L. Structural similarity index (SSIM) revisited: A data-driven approach. Expert Syst Appl. 2022;189:116087.

45. Setiadi DIM. PSNR vs SSIM: Imperceptibility quality assessment for image steganography. Multimed Tools Appl. 2021;80:8423–44.

46. Parent JR, Witharana C, Bradley M. Classifying and georeferencing indoor point clouds with arcgis. Photogramm Eng Remote Sens. 2022;88:383–9.

47. Zuo RG, Wang JL. ArcFractal: An arcgis add-in for processing geoscience data using fractal/multifractal models. Nat Resour Res. 2020;29:3–12.

48. Singh S, Mittal N, Singh H, Oliva D. Improving the segmentation of digital images by using a modified Otsu's between-class variance. Multimed Tools Appl. 2023;82:40701–43.

49. Xing JW, Yang P, Qingge LG. Robust 2D Otsu's Algorithm for Uneven Illumination Image Segmentation. Comput Intell Neurosci. 2020;2020:5047976.

50. Wu B, Zhou JX, Ji XY, Yin YJ, Shen X. An ameliorated teaching-learning-based optimization algorithm based study of image segmentation for multilevel thresholding using Kapur's entropy and Otsu's between class variance. Inf Sci. 2020;533:72–107.

51. Zhu HL, Huang YW, An ZK, Zhang H, Han YY, Zhao ZH, et al. Assessing radiometric calibration methods for multispectral UAV imagery and the influence of illumination, flight altitude and flight time on reflectance, vegetation index and inversion of winter wheat AGB and LAI. Comput Electron Agric. 2024;219:108821.

52. Tan CY, Chen ZJ, Liao AL, Zeng XT, Cao JC. Accuracy analysis of UAV aerial photogrammetry based on RTK mode, flight altitude, and number of GCPs. Meas Sci Technol. 2024;35:106310.

53. Gu YY, Wang YQ, Guo T, Guo CL, Wang X, Jiang CY, et al. Assessment of the influence of UAV-borne LiDAR scan angle and flight altitude on the estimation of wheat structural metrics with different leaf angle distributions. Comput Electron Agric. 2024;220:108858.

© 2023 The Author(s). | Published by Agro Intelligence Research Press